DESY 15-073

Improved prediction for the mass of the W boson in the NMSSM

O. Stål[1,*], G. Weiglein[2,†], L. Zeune[3‡]

[1] *The Oskar Klein Centre, Department of Physics*
Stockholm University, SE-106 91 Stockholm, Sweden

[2] *Deutsches Elektronen-Synchrotron DESY*
Notkestraße 85, D-22607 Hamburg, Germany

[3] *ITFA, University of Amsterdam*
Science Park 904, 1018 XE, Amsterdam, The Netherlands

Abstract

Electroweak precision observables, being highly sensitive to loop contributions of new physics, provide a powerful tool to test the theory and to discriminate between different models of the underlying physics. In that context, the W boson mass, M_W, plays a crucial role. The accuracy of the M_W measurement has been significantly improved over the last years, and further improvement of the experimental accuracy is expected from future LHC measurements. In order to fully exploit the precise experimental determination, an accurate theoretical prediction for M_W in the Standard Model (SM) and extensions of it is of central importance. We present the currently most accurate prediction for the W boson mass in the Next-to-Minimal Supersymmetric extension of the Standard Model (NMSSM), including the full one-loop result and all available higher-order corrections of SM and SUSY type. The evaluation of M_W is performed in a flexible framework, which facilitates the extension to other models beyond the SM. We show numerical results for the W boson mass in the NMSSM, focussing on phenomenologically interesting scenarios, in which the Higgs signal can be interpreted as the lightest or second lightest $\mathcal{CP}$-even Higgs boson of the NMSSM. We find that, for both Higgs signal interpretations, the NMSSM M_W prediction is well compatible with the measurement. We study the SUSY contributions to M_W in detail and investigate in particular the genuine NMSSM effects from the Higgs and neutralino sectors.

*Electronic address: oscar.stal@fysik.su.se
†Electronic address: Georg.Weiglein@desy.de
‡Electronic address: l.k.zeune@uva.nl

1 Introduction

Supersymmetry (SUSY) is regarded to be the most appealing extension of the Standard Model (SM), as it provides a natural mechanism to explain a light Higgs boson as observed by ATLAS [1] and CMS [2]. Supersymmetry realised around the TeV-scale also comes with further desirable features, such as a possible dark matter candidate and the unification of gauge couplings.

The superpotential of the Minimal Supersymmetric extension of the Standard Model (MSSM) contains a term bilinear in the two Higgs doublets, $W_{(2)} \sim \mu H_2 H_1$. In this term a dimensionful parameter, μ, is present, which in the MSSM has no natural connection to the SUSY breaking scale. The difficulty to motivate a phenomenologically acceptable value in this context is called the μ-problem of the MSSM [3]. This problem is addressed in the Next-to-Minimal Supersymmetric extension of the Standard Model (NMSSM), where the Higgs sector of the MSSM gets enlarged by an additional singlet. The corresponding term in the superpotential is replaced by a coupling $W_{(3)} \sim \lambda S H_2 H_1$, and the μ parameter arises dynamically from the vev of the singlet, S, and may therefore be related to the SUSY breaking scale.

Besides the solution of the μ-problem, there are additional motivations to study the NMSSM. The physical spectrum contains seven Higgs bosons, which leads to a rich and interesting phenomenology. Compared to the MSSM, the singlet field modifies the Higgs mass relations such that the tree-level mass of the lightest neutral Higgs boson can be increased. Consequently, the radiative corrections needed to shift the mass of the lightest Higgs mass up to 125 GeV can be smaller. This relaxes the requirement of heavy stops, or a large splitting in the stop sector, in NMSSM parameter regions where the tree-level Higgs mass is larger than the maximal MSSM value (see e.g. Ref. [4]). The NMSSM singlet-doublet mixing could also modify the couplings of the 125 GeV boson to explain a potentially enhanced rate in the diphoton signal (see e.g. Refs. [5–8]).

Extensive direct searches for supersymmetric particles are carried out by the LHC experiments. These searches have so far not resulted in a signal, which leads to limits on the particle masses, see e.g. Refs. [9–11] for a compilation of the results. Indirect methods are complementary to direct searches for physics beyond the SM at the LHC and future collider experiments. Whereas direct methods attempt to observe traces in the detectors arising from of the direct production of particles of new physics models, indirect methods look for the quantum effects induced by virtual exchange of new states. Even if not yet seen directly, signs of new physics may show up as small deviations between precise measurements and SM predictions. Electroweak precision observables (EWPOs), such as the W boson mass, M_W, the sine of the effective leptonic weak mixing angle at the Z boson resonance, $\sin^2\theta_{\mathrm{w}}^{\mathrm{eff}}$, or the anomalous magnetic moment of the muon, $(g-2)_\mu$, (among others) are all highly sensitive to loop contributions involving in principle all the particles of the considered model. They can both be theoretically predicted and experimentally measured with such a high precision that they can be utilised to test the SM, to distinguish between different extensions, and to derive indirect constraints on the parameters of a model. Input from indirect methods can be of great interest to direct searches for new particles. This was demonstrated, for instance, by the discovery of the top quark with a measured mass in remarkable agreement with the indirect prediction [12, 13].

In this paper we focus on the W boson mass. The accuracy of the measurement of M_W has been significantly improved in the last years with the results presented by the Tevatron experiments CDF [14] and DØ [15]. The current world average is [16, 17]

$$M_W^{\mathrm{exp}} = 80.385 \pm 0.015 \text{ GeV}. \tag{1}$$

This precise measurement makes M_W particularly suitable for electroweak precision tests, even more

since the precision is expected to be improved further when including the full dataset from the Tevatron and upcoming results from the LHC. Of central importance for the theoretical precision that can be achieved on M_W is the top quark mass measurement, since the experimental error on the input parameter m_t constitutes a dominant source of (parametric) uncertainty, see e.g. Ref. [18]. The Tevatron [19] and LHC [20–26] measurements of m_t have been combined [27] to yield

$$m_t^{\rm exp} = 173.34 \pm 0.27 \pm 0.71 \text{ GeV}. \tag{2}$$

In contrast to the M_W measurement, a considerable improvement of the precision on m_t beyond Eq. (2) seems less likely at the LHC. Furthermore, it is not straightforward to relate $m_t^{\rm exp}$ measured at a hadron collider (using kinematic information about the top decay products) to a theoretically well-defined mass parameter. The quantity measured with high precision at the Tevatron and the LHC is expected to be close to the top pole mass with an uncertainty at the level of about 1 GeV [28–30]. For the calculation of M_W presented in this paper we adopt the interpretation of the measured value $m_t^{\rm exp}$ as the pole mass, but the results could easily be re-expressed in terms of a properly defined short distance mass (such as the $\overline{\rm MS}$ or $\overline{\rm DR}$ mass). At an e^+e^- linear collider, the situation would improve significantly. Estimates for the ILC show an expected precision $\Delta M_W^{\rm ILC} \sim 2.5 - 5$ MeV and $\Delta m_t^{\rm ILC} = 0.1$ GeV [31, 32], where the stated precision for m_t accounts both for the uncertainty in the determination of the actually measured mass parameter and the uncertainty related to the conversion into a suitable and theoretically well-defined parameter such as the $\overline{\rm MS}$ mass.

For exploiting the precise current and (possible) future M_W measurements, theoretical predictions for M_W with comparable accuracy are desired both in the SM and extensions of it. In order to be able to discriminate between different models it is necessary that the precision is comparable. In the SM, the most advanced evaluation of M_W includes the full one-loop [33, 34] and two-loop [35–47] result, as well as the leading three- and four-loop corrections [48–57]. A simple parametrization for $M_W^{\rm SM}$ has also been developed [58], see also Ref. [59]. Within the SM the LHC Higgs signal at 125.09 GeV [60] is interpreted as the SM Higgs boson. Setting $M_H^{\rm SM} \simeq 125.09$ GeV, the value of M_W can be predicted in the SM without any free parameters. The result (for $m_t = 173.34$ GeV, $M_H^{\rm SM} = 125.09$ GeV) is[1]

$$M_W^{\rm SM} = 80.358 \text{ GeV}, \tag{3}$$

which differs by $\sim 1.8\,\sigma$ from the experimental value given in Eq. (1). The theoretical uncertainty from missing higher-order corrections has been estimated to be around 4 MeV in the SM for a light Higgs boson [58].

For supersymmetric theories, the one-loop result for M_W [62–73] and leading two-loop corrections [74–77] have been obtained for the MSSM. A precise prediction for $M_W^{\rm MSSM}$, taking into account all relevant higher-order corrections of both SM- and SUSY-type, was presented in Ref. [61]. A first prediction for M_W in the NMSSM has also been presented in Ref. [78]. For the study of other EWPOs (mainly focusing on Z decays) in the NMSSM, see Refs. [78–80].

In this work we follow the procedure employed in the MSSM to present a new prediction for M_W in the NMSSM with the same level of accuracy as the current best MSSM prediction [61]. We combine the complete NMSSM one-loop result with the state-of-the-art SM result and leading SUSY higher-order corrections. Our framework allows to output, besides M_W, also the quantity Δr directly (see Sect. 3), which summarises all (non-QED) quantum correction to the muon decay amplitude. Besides its importance for electroweak precision tests, Δr is needed whenever a theoretical prediction

[1] We updated the SM M_W prediction as discussed below in Sect. 4.3. This leads to a small difference compared to the SM value given in Ref. [61].

is parametrized in terms of the Fermi constant G_μ (instead of M_W or $\alpha(M_Z)$). Our NMSSM prediction for M_W provides the flexibility to analyse SUSY loop contributions analytically and to treat possible threshold effects or numerical instabilities. We perform a detailed numerical analysis of M_W in the NMSSM with the latest experimental results taken into account. We focus on the effects induced by the extended Higgs and neutralino sectors, and in particular on benchmark scenarios where the LHC Higgs boson is interpreted as either the lightest or the second lightest $\mathcal{CP}$-even Higgs boson of the NMSSM.

This paper is organised as follows: in Sect. 2 we give a short introduction to the NMSSM, focussing on the Higgs and neutralino sectors. In Sect. 3 we describe the determination of the W boson mass in the NMSSM. We outline the calculation of the one-loop contributions and the incorporation of higher-order contributions. In Sect. 4 we give the numerical results, analysing the NMSSM contributions to the W boson mass, before we conclude in Sect. 5.

2 The Next-to-Minimal Supersymmetric Standard Model

In this section we introduce the NMSSM and specify our notation. We focus on the particle sectors which differ from the MSSM. Since the SM fermions and their superpartners appear in the same way in both models, the sfermion sector of the NMSSM is unchanged with respect to the MSSM. Also the chargino sector is identical to that in the MSSM since no new charged degrees of freedom are introduced. For these sectors we use the same notation as employed in Ref. [61].

In addition to the two Higgs doublets of the MSSM, the NMSSM also contains a Higgs singlet, S, which couples only to the Higgs sector.[2] Considering the Z_3-symmetric version of the NMSSM, the superpotential takes the form

$$W^{\rm NMSSM} = \bar{u}\mathbf{y}_u Q H_2 - \bar{d}\mathbf{y}_d Q H_1 - \bar{e}\mathbf{y}_l L H_1 + \lambda S H_2 H_1 + \frac{1}{3}\kappa S^3\,. \tag{4}$$

The new contributions of the Higgs singlet to the soft breaking terms are

$$\mathcal{L}_{\rm soft}^{\rm NMSSM} = \mathcal{L}_{\rm soft}^{\rm MSSM,mod} - m_S^2|S|^2 - (\lambda A_\lambda S H_2 H_1 + \frac{1}{3}\kappa A_\kappa S^3 + \text{h.c.}), \tag{5}$$

where $\mathcal{L}_{\rm soft}^{\rm MSSM,mod}$ is the soft-breaking Lagrangian $\mathcal{L}_{\rm soft}^{\rm MSSM}$ of the MSSM (see e.g. Eq. (6.3.1) of Ref. [81]), but without the term bH_2H_1. The singlet couplings make it possible to dynamically generate an effective μ parameter as

$$\mu_{\rm eff} = \lambda\langle S\rangle. \tag{6}$$

The additional contributions (and the modified effective μ term) in the superpotential and in the soft breaking terms lead to a Higgs potential which contains the additional soft breaking parameters m_S^2, A_λ, A_κ, as well as the superpotential trilinear couplings λ and κ. Like in the MSSM, there is no $\mathcal{CP}$-violation at tree-level in the couplings of the Higgs doublets. The new doublet-singlet couplings allow in principle for $\mathcal{CP}$-violation at tree level, but we will not consider this possibility here. We choose all parameters to be real.

The minimum of the NMSSM Higgs potential triggers electroweak symmetry breaking, after which the Higgs doublets can be expanded around their minima according to

$$H_1 = \begin{pmatrix} v_1 + \frac{1}{\sqrt{2}}(\phi_1 - \mathrm{i}\chi_1) \\ -\phi_1^- \end{pmatrix}, \qquad H_2 = \begin{pmatrix} \phi_2^+ \\ v_2 + \frac{1}{\sqrt{2}}(\phi_2 + \mathrm{i}\chi_2) \end{pmatrix}. \tag{7}$$

[2] For the Higgs doublets and the Higgs singlet we use the same notation for the supermultiplets and for its scalar component.

Similarly, the singlet scalar component can be expanded as

$$S = v_s + \frac{1}{\sqrt{2}}\left(\phi_s + \mathrm{i}\chi_s\right), \tag{8}$$

where v_s is the (non-zero) vacuum expectation value of the singlet.

The bilinear part of the Higgs potential can be written as

$$\begin{aligned} V_H = \tfrac{1}{2}\left(\phi_1,\phi_2,\phi_S\right)\mathbf{M}_{\phi\phi\phi}\begin{pmatrix}\phi_1\\ \phi_2\\ \phi_S\end{pmatrix} + \tfrac{1}{2}\left(\chi_1,\chi_2,\chi_S\right)\mathbf{M}_{\chi\chi\chi}\begin{pmatrix}\chi_1\\ \chi_2\\ \chi_S\end{pmatrix} \\ + \left(\phi_1^-,\phi_2^-\right)\mathbf{M}_{\phi^\pm\phi^\pm}\begin{pmatrix}\phi_1^+\\ \phi_2^+\end{pmatrix} + \cdots, \end{aligned} \tag{9}$$

with the mass matrices $\mathbf{M}_{\phi\phi\phi}$, $\mathbf{M}_{\chi\chi\chi}$ and $\mathbf{M}_{\phi^\pm\phi^\pm}$.

The mixing of the $\mathcal{CP}$-even, $\mathcal{CP}$-odd and charged Higgs fields occurring in the mass eigenstates is described by three unitary matrices U^H, U^A, and U^C, where

$$\begin{pmatrix}h_1\\ h_2\\ h_3\end{pmatrix} = U^H\begin{pmatrix}\phi_1\\ \phi_2\\ \phi_S\end{pmatrix}, \quad \begin{pmatrix}a_1\\ a_2\\ G\end{pmatrix} = U^A\begin{pmatrix}\chi_1\\ \chi_2\\ \chi_S\end{pmatrix}, \quad \begin{pmatrix}H^\pm\\ G^\pm\end{pmatrix} = U^C\begin{pmatrix}\phi_1^\pm\\ \phi_2^\pm\end{pmatrix}. \tag{10}$$

These transform the Higgs fields such that the resulting (diagonal) mass matrices become

$$\mathbf{M}^{\text{diag}}_{hhh} = U^H\mathbf{M}_{\phi\phi\phi}\left(U^H\right)^\dagger,\ \mathbf{M}^{\text{diag}}_{aaG} = U^A\mathbf{M}_{\chi\chi\chi}\left(U^A\right)^\dagger \text{ and } \mathbf{M}^{\text{diag}}_{H^\pm G^\pm} = U^C\mathbf{M}_{\phi^\pm\phi^\pm}\left(U^C\right)^\dagger \tag{11}$$

The $\mathcal{CP}$-even mass eigenstates, h_1, h_2 and h_3, are ordered such that $m_{h_1} \leq m_{h_2} \leq m_{h_3}$, and similarly for the two $\mathcal{CP}$-odd Higgs bosons, a_1 and a_2. Unchanged from the SM there are also the Goldstone bosons, G and $G^\pm$. Finally, there is the charged Higgs pair, $H^\pm$ with mass given by

$$M^2_{H^\pm} = \hat{m}^2_A + M^2_W - \lambda^2 v^2. \tag{12}$$

Here $\hat{m}_A$ is the effective $\mathcal{CP}$-odd doublet mass given by

$$\hat{m}^2_A = \frac{\lambda v_s}{\sin\beta\,\cos\beta}\left(A_\lambda + \kappa v_s\right). \tag{13}$$

The superpartner of the singlet scalar enlarging the NMSSM Higgs sector is called the singlino, $\tilde{S}$. It extends the neutralino sector with a fifth mass eigenstate. In the basis $(\tilde{B},\tilde{W}^0,\tilde{H}^0_1,\tilde{H}^0_2,\tilde{S})$ the neutralino mass matrix at tree level is given by

$$\mathbf{M}_{\tilde{\chi}^0} = \begin{pmatrix} M_1 & 0 & -M_Z s_W\cos\beta & M_Z s_W\sin\beta & 0 \\ 0 & M_2 & M_Z c_W\cos\beta & -M_Z c_W\sin\beta & 0 \\ -M_Z s_W\cos\beta & M_Z c_W\cos\beta & 0 & -\mu_{\text{eff}} & -\lambda v_2 \\ M_Z s_W\sin\beta & -M_Z c_W\sin\beta & -\mu_{\text{eff}} & 0 & -\lambda v_1 \\ 0 & 0 & -\lambda v_2 & -\lambda v_1 & 2K\mu_{\text{eff}} \end{pmatrix}, \tag{14}$$

where $K \equiv \kappa/\lambda$. This mass matrix can be diagonalised by a single unitary matrix N such that

$$\text{diag}(m_{\tilde{\chi}^0_1}, m_{\tilde{\chi}^0_2}, m_{\tilde{\chi}^0_3}, m_{\tilde{\chi}^0_4}, m_{\tilde{\chi}^0_5}) = N^*\mathbf{M}_{\tilde{\chi}^0}N^\dagger, \tag{15}$$

which gives the mass eigenvalues ordered as $m_{\tilde{\chi}^0_i} \leq m_{\tilde{\chi}^0_j}$ for $i < j$.

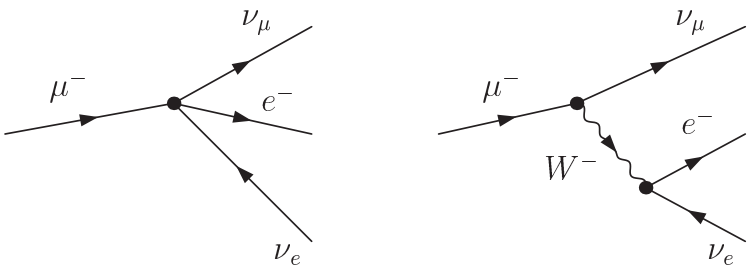

Figure 1: Left: tree-level diagram with a four-fermion vertex describing muon decay in the Fermi model. Right: W boson exchange mediating muon decay in the electroweak SM (in unitary gauge).

3 Predicting the W boson mass

3.1 Determination of M_W

The W boson mass can theoretically be predicted from the muon decay rate. Muons decay to almost 100% via $\mu \to e\bar{\nu}_e\nu_\mu$ [82]. This decay was historically described first within the Fermi model (left diagram in Fig. 1). Comparing the muon decay amplitude calculated in the Fermi model to the same quantity calculated in the full SM or extensions thereof (the leading-order contribution in unitary gauge is depicted in Fig. 1) yields the relation

$$\frac{G_\mu}{\sqrt{2}} = \frac{M_Z^2\, e^2}{8\, M_W^2\, \left(M_Z^2 - M_W^2\right)} \left(1 + \Delta r(M_W, M_Z, m_t, \, ..., X)\right). \tag{16}$$

This relates the W boson mass to the Fermi constant, G_μ, which by definition contains the QED corrections to the four-fermion contact vertex up to $O(\alpha^2)$ [83–87], and to the other parameters M_Z and e, which are known experimentally with very high precision. The Fermi constant itself is determined with high accuracy from precise measurements of the muon life time [88].

The factor Δr in Eq. (16) summarises all higher-order contributions to the muon decay amplitude after subtracting the Fermi-model type virtual QED corrections, which are already included in the definition of G_μ. Working in the on-shell renormalization scheme, Eq. (16) corresponds to a relation between the physical masses of the W and Z bosons.

Neglecting the masses and momenta of the external fermions all loop diagrams can be expressed as a term proportional to the Born matrix element [33, 43]

$$\mathcal{M}_{\text{Loop,i}} = \Delta r_i \; \mathcal{M}_{\text{Born}}\,, \quad \Delta r = \sum_i \Delta r_i\,. \tag{17}$$

In different models, different particles can contribute as virtual particles in the loop diagrams to the muon-decay amplitude. Therefore, the quantity Δr depends on the specific model parameters (indicated by the X in Eq. (16)), and Eq. (16) provides a model-dependent prediction for the W boson mass. The quantity Δr itself does depend on M_W as well; hence, the value of M_W as the solution of Eq. (16) has to be determined numerically. In practice this is done by iteration.

In order to exploit the W boson mass for electroweak precision tests a precise theoretical prediction for Δr within and beyond the SM is needed. In the next two subsections we describe our calculation of Δr in the NMSSM. A new one-loop calculation has been performed which is combined with all available higher order corrections of SM- and SUSY-type.

3.2 One-loop calculation of Δr in the NMSSM

The one-loop contributions to Δr consist of the W boson self-energy, vertex and box diagrams, and the corresponding counter terms (CT). The box diagrams are themselves UV-finite in a renormalizable gauge and require no counter terms. Schematically, this can be expressed as

$$\begin{aligned}\Delta r^{(\alpha)} &= W \text{ Self-energy} + W \text{ Self-energy CT} + \text{Vertex} + \text{Vertex CT} + \text{Box} \\ &= \frac{\Sigma_T^{WW}(0)}{M_W^2} + \left(-\delta Z_W - \frac{\delta M_W^2}{M_W^2}\right) + \text{Vertex} \\ &+ \left(2\delta e - 2\frac{\delta s_\mathrm{w}}{s_\mathrm{w}} + \delta Z_W + \frac{1}{2}\left(\delta Z^\mu + \delta Z^e + \delta Z^{\nu_\mu} + \delta Z^{\nu_e}\right)\right) + \text{Box}\,.\end{aligned} \tag{18}$$

Here $\Sigma_T^{WW}(0)$ denotes the transverse part the W boson self-energy (evaluated at vanishing momentum transfer), δM_W is the renormalization constant for the W boson mass, δe and δs_w are the renormalization constants for the electric charge and $s_\mathrm{w} \equiv \sin\theta_W$, respectively. The δZ denote different field renormalization constants. Since the W boson occurs in the muon decay amplitude only as a virtual particle, its field renormalization constant δZ_W cancels in the expression for Δr.

We employ the on-shell renormalization scheme. The one-loop renormalization constants of the W and Z boson masses are then given by

$$M^2_{W/Z,0} = M^2_{W/Z} + \delta M^2_{W/Z}\,, \quad \delta M^2_{W/Z} = \mathrm{Re}\,\Sigma_T^{WW/ZZ}(M^2_{W/Z}), \tag{19}$$

where bare quantities are denoted with a zero subscript. The renormalization constant of the electric charge is

$$e_0 = (1+\delta e)e\,, \quad \delta e = \frac{1}{2}\Pi^{AA}(0) + \frac{s_\mathrm{w}}{c_\mathrm{w}}\frac{\Sigma_T^{AZ}(0)}{M_Z^2}\,, \tag{20}$$

with

$$\Pi^{AA}(k^2) = \frac{\Sigma_T^{AA}(k^2)}{k^2}\,, \quad \Pi^{AA}(0) = \frac{\partial\Sigma_T^{AA}(k^2)}{\partial k^2}|_{k^2=0}. \tag{21}$$

Note that the sign appearing in front of s_w in Eq. (20) depends on convention chosen for the $SU(2)$ covariant derivative.[3] The sine of the weak mixing angle is not an independent parameter in the on-shell renormalization scheme. Its renormalization constant

$$s_{\mathrm{w},0} = s_\mathrm{w} + \delta s_\mathrm{w}\,, \quad \frac{\delta s_\mathrm{w}}{s_\mathrm{w}} = -\frac{1}{2}\frac{c_\mathrm{w}^2}{s_\mathrm{w}^2}\mathrm{Re}\left(\frac{\Sigma_T^{WW}(M_W^2)}{M_W^2} - \frac{\Sigma_T^{ZZ}(M_Z^2)}{M_Z^2}\right) \tag{22}$$

is fixed by the renormalization constants of the weak gauge boson masses.

Finally, the renormalization constant of a (left-handed) lepton field l (neglecting the lepton mass) is

$$l_0^L = \left(1 + \frac{1}{2}\delta Z^{l,L}\right) l^L\,, \quad \delta Z^{l,L} = -\Sigma_L^l(0)\,, \tag{23}$$

where Σ_L^l denotes the left-handed part of the lepton self energy.

[3] We adopt the sign conventions for the $SU(2)_L$ covariant derivative used in the code `FeynArts` [89–94], where (for historical reasons) the $SU(2)_L$ covariant derivative is defined by $\partial_\mu - \mathrm{i}g_2 I^a W_\mu^a$ for the SM and $\partial_\mu + \mathrm{i}g_2 I^a W_\mu^a$ for the (N)MSSM. The expressions given here correspond to the (N)MSSM convention.

Inserting these expressions for the renormalisation constants into Eq. (18) yields

$$\begin{aligned}\Delta r^{(\alpha)} =& \frac{\Sigma_T^{WW}(0) - \mathrm{Re}\left[\Sigma_T^{WW}(M_W^2)\right]}{M_W^2} + \Pi^{AA}(0) - \frac{c_\mathrm{w}^2}{s_\mathrm{w}^2}\,\mathrm{Re}\left[\frac{\Sigma_T^{ZZ}(M_Z^2)}{M_Z^2} - \frac{\Sigma_T^{WW}(M_W^2)}{M_W^2}\right] \\ &+ 2\,\frac{s_\mathrm{w}}{c_\mathrm{w}}\frac{\Sigma_T^{AZ}(0)}{M_Z^2} + \mathrm{Vertex} + \mathrm{Box} - \frac{1}{2}\left(\Sigma_L^e(0) + \Sigma_L^\mu(0) + \Sigma_L^{\nu_e}(0) + \Sigma_L^{\nu_\mu}(0)\right).\end{aligned} \tag{24}$$

The quantity Δr is at one loop level conventionally split into three parts,

$$\Delta r^{(\alpha)} = \Delta\alpha - \frac{c_\mathrm{w}^2}{s_\mathrm{w}^2}\Delta\rho + \Delta r_\mathrm{rem}. \tag{25}$$

The shift of the fine structure constant $\Delta\alpha$ arises from the charge renormalization which contains the contributions from light fermions. The quantity $\Delta\rho$ contains loop corrections to the ρ parameter [95], which describes the ratio between neutral and charged weak currents, and can be written as

$$\Delta\rho = \frac{\Sigma_T^{ZZ}(0)}{M_Z^2} - \frac{\Sigma_T^{WW}(0)}{M_W^2}\,. \tag{26}$$

This quantity is sensitive to the mass splitting between the isospin partners in a doublet [95], which leads to a sizeable effect in the SM in particular from the heavy quark doublet. While $\Delta\alpha$ is a pure SM contribution, $\Delta\rho$ can get large contributions also from SUSY particles, in particular the superpartners of the heavy quarks. All other terms, both of SM and SUSY type, are contained in the remainder term Δr_rem.

We have performed a diagrammatic one-loop calculation of Δr in the NMSSM according to Eq. (24), using the `Mathematica`-based programs `FeynArts` [89–94] and `FormCalc` [96]. The NMSSM model file for `FeynArts`, first used in [6], has been adapted from output from `SARAH` [97, 98].

The calculation of the SM-type diagrams (being part of the NMSSM contributions) are not discussed here. This calculation has been discussed in the literature already many years ago [33, 34], and we refer to Refs. [43, 99] for details. The one-loop result for Δr is also known for the MSSM (with complex parameters), see Refs. [61, 73]. The calculation in the NMSSM follows along the same lines as for the MSSM. However, the result gets modified from differences in the Higgs and the neutralino sectors. Below we outline the NMSSM one-loop contributions to Δr, for completeness also including the MSSM-type contributions.

Besides the SM-type contributions with fermions and gauge bosons in the loops (not discussed further here), many additional self-energy, vertex and box diagrams appear in the NMSSM with sfermions, (SUSY) Higgs bosons, charginos and neutralinos in the loop. Generic examples of gauge-boson self-energy diagrams with sfermions are depicted in Fig. 2. Their contribution to Δr is finite by itself. The NMSSM Higgs bosons enter only in gauge boson self-energy diagrams, since we have neglected the masses of the external fermions. The contributing diagrams are sketched in Fig. 3. These contributions are not finite by themselves. Only if one considers all (including SM-type) gauge boson and Higgs contributions to the gauge boson self-energy diagrams, the vertex diagrams and vertex counterterm diagrams together, the divergences cancel, and one finds a finite result.

Charginos and neutralinos enter in gauge boson self-energy diagrams (depicted in Fig. 4), fermion self-energy diagrams (depicted in Fig. 5), vertex diagrams (depicted in Fig. 6, the analogous vertex corrections exist also for the other vertex) and box diagrams (depicted in Fig. 7). The vertex contributions from the chargino/neutralino sector, together with the chargino/neutralino contributions to the vertex CT and the gauge boson self-energies are finite. Each box diagram is UV-finite by itself.

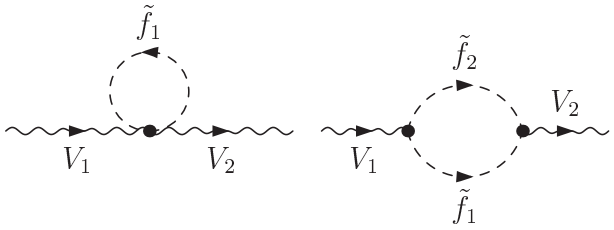

Figure 2: Generic (N)MSSM one-loop gauge boson self-energy diagrams with a sfermion loop; V_1, V_2 = γ, Z, $W^\pm$ and $\tilde{f}_1$, $\tilde{f}_2 = \tilde{\nu}$, $\tilde{l}$, $\tilde{u}$, $\tilde{d}$.

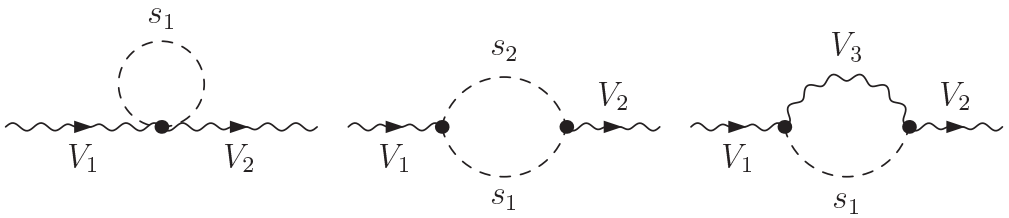

Figure 3: Generic NMSSM one-loop gauge boson self-energy diagrams with gauge bosons, Higgs and Goldstone bosons in the loop; V_1, V_2, $V_3 = \gamma$, Z, $W^\pm$ and s_1, $s_2 = h_1$, h_2, h_3, a_1, a_2, $H^\pm$, G, $G^\pm$.

In order to determine the contribution to Δr from a particular loop diagram, the Born amplitude has to be factored out of the one-loop muon decay amplitude, as shown in Eq. (17). While most loop diagrams directly give a result proportional to the Born amplitude, more complicated spinor structures that do not occur in the SM case arise from box diagrams containing neutralinos and charginos[4]. Performing the calculation of the box diagrams in Fig. 7 in `FormCalc`, the spinor chains are returned in the form

$$\begin{aligned}
\mathcal{M}_{\text{SUSY Box}(a)} &= (\bar{u}_e \gamma_\lambda \omega_- u_\mu)(\bar{u}_{\nu_\mu} \gamma^\lambda \omega_- v_{\nu_e}) b_{(a)} \\
\mathcal{M}_{\text{SUSY Box}(b)} &= (\bar{u}_{\nu_e} \omega_- u_\mu)(\bar{u}_{\nu_\mu} \omega_+ v_e) b_{(b)} \; .
\end{aligned} \tag{27}$$

The expressions for the coefficients $b_{(a)}$ and $b_{(b)}$ are lengthy and not given here explicitly. In order to factor out the Born amplitude

$$\mathcal{M}_{\text{Born}} = \frac{2\pi\alpha}{s_\text{w}^2 M_W^2} \left(\bar{u}_{\nu_\mu} \gamma_\lambda \omega_- u_\mu\right) \left(\bar{u}_e \gamma^\lambda \omega_- v_{\nu_e}\right) , \tag{28}$$

the spinor chains in Eq. (27) have to be transformed into the same structure. We modify the spinor chains following the procedure described in Ref. [73] and get

$$\begin{aligned}
\mathcal{M}_{\text{SUSY Box}(a)} &= -\frac{s_\text{w}^2 M_W^2}{2\pi\alpha} \, b_{(a)} \, \mathcal{M}_{\text{Born}} \\
\mathcal{M}_{\text{SUSY Box}(b)} &= \frac{s_\text{w}^2 M_W^2}{4\pi\alpha} \, b_{(b)} \, \mathcal{M}_{\text{Born}} \; .
\end{aligned} \tag{29}$$

The coefficients $b_{(a)}$ and $b_{(b)}$ contain ratios of mass-squared differences of the involved particles. These coefficients can give rise to numerical instabilities in cases of mass degeneracies. In the implementation of our results (which has been carried out in a `Mathematica`) special care has been taken of

[4]The same complication occurs in the MSSM and was discussed in Ref. [73].

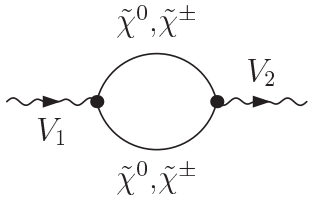

Figure 4: Generic NMSSM one-loop gauge boson self-energy diagram with charginos/neutralinos; V_1, $V_2 = \gamma$, Z, $W^\pm$, $\tilde{\chi}^\pm = \tilde{\chi}^\pm_{1,2}$ and $\tilde{\chi}^0 = \tilde{\chi}^0_{1,2,3,4,5}$.

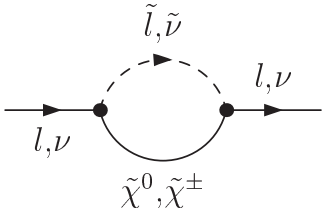

Figure 5: Generic NMSSM one-loop fermion self-energy diagram with a chargino/neutralino/sfermion contribution; $\tilde{\chi}^\pm = \tilde{\chi}^\pm_{1,2}$ and $\tilde{\chi}^0 = \tilde{\chi}^0_{1,2,3,4,5}$.

such parameter regions with mass degeneracies or possible threshold effects. By adding appropriate expansions a numerically stable evaluation is ensured.

3.3 Higher-order corrections

The on-shell renormalization conditions correspond to the definition of the W and Z boson masses according to the real part of the complex pole of the propagator, which from two-loop order on is the only gauge-invariant way to define the masses of unstable particles (see Ref. [43] and references therein). The expansion around the complex pole results in a Breit-Wigner shape with a fixed width (fw). Internally we therefore use this definition (fw) of the gauge boson masses. The experimentally measured values of the gauge boson masses are obtained using a mass definition in terms of a Breit-Wigner shape with a running width (rw). As the last step of our calculation, we therefore transform the W boson mass value to the running width definition, $M_W^{\rm rw}$ to facilitate a direct comparison to the experimental value of M_W. The difference between these two definitions is

$$M_W^{\rm rw} = M_W^{\rm fw} + \frac{\Gamma_W^2}{2M_W^{\rm rw}}, \tag{30}$$

where $M_W^{\rm fw}$ corresponds to the fixed width description, see Ref. [100]. For the prediction of the W decay width we use

$$\Gamma_W = \frac{3G_\mu \left(M_W^{\rm rw}\right)^3}{2\sqrt{2}\pi} \left(1 + \frac{2\alpha_s}{3\pi}\right), \tag{31}$$

parametrized by G_μ and including first order QCD corrections. The difference between the fixed- and running width definitions amounts to about 27 MeV, which is very relevant in view of the current theoretical and experimental precisions. For the Z boson mass, which is used as an input parameter in the prediction for M_W, the conversion from the running-width to the fixed-width definition is carried

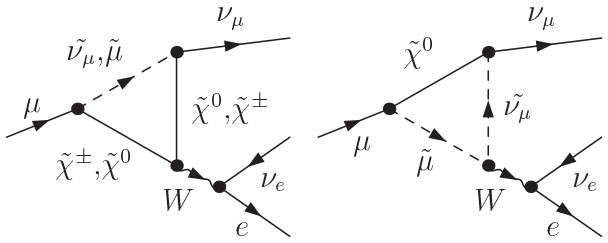

Figure 6: Generic one-loop vertex correction diagrams in the NMSSM; $\tilde{\chi}^\pm = \tilde{\chi}^\pm_{1,2}$ and $\tilde{\chi}^0 = \tilde{\chi}^0_{1,2,3,4,5}$. Analoguous diagrams exist for the other W vertex.

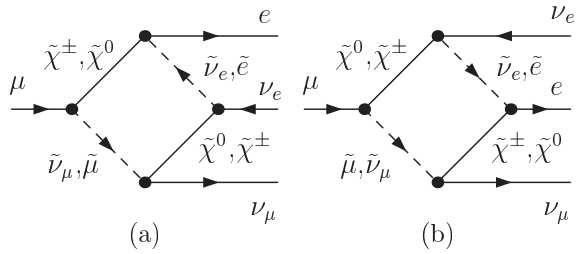

Figure 7: Generic one-loop box diagrams contributing to the muon decay amplitude in the NMSSM; $\tilde{\chi}^\pm = \tilde{\chi}^\pm_{1,2}$ and $\tilde{\chi}^0 = \tilde{\chi}^0_{1,2,3,4,5}$.

out in the first step of the calculation. Accordingly, keeping track of the proper definition of the gauge boson masses is obviously important in the context of electroweak precision physics. For the remainder of this paper we will not use the labels (rw, fw) explicitly; if we do not refer to an internal variable, M_W and M_Z will always refer to the mass definition according to a Breit-Wigner shape with a *running* width (see e.g. Ref. [43] for further details; see also Refs. [101, 102]).

We combine the SM one-loop result (which is part of the NMSSM calculation) with the relevant available higher-order corrections of the state-of-the-art prediction for $M_W^{\rm SM}$. As we will describe below in more detail, the higher-order corrections of SM-type are also incorporated in the NMSSM calculation of Δr in order to achieve an accurate prediction for $M_W^{\rm NMSSM}$. For a discussion of the incorporation of higher-order contributions to M_W in the MSSM see Refs. [61, 73].

In a first step, we write the NMSSM result for Δr as the sum of the full one-loop and the higher-order corrections,

$$\Delta r^{\rm NMSSM} = \Delta r^{\rm NMSSM(\alpha)} + \Delta r^{\rm NMSSM(h.o.)}, \tag{32}$$

where $\Delta r^{\rm NMSSM(\alpha)}$ denotes the NMSSM one-loop contributions from the various particle sectors

$$\Delta r^{\rm NMSSM(\alpha)} = \Delta r^{\rm fermion(\alpha)} + \Delta r^{\rm gauge\text{-}boson/Higgs(\alpha)} + \Delta r^{\rm sfermion(\alpha)} + \Delta r^{\rm chargino/neutralino(\alpha)}, \tag{33}$$

as discussed in the previous subsection. The term $\Delta r^{\rm NMSSM(h.o.)}$ denotes the higher-oder contributions, which we split into a SM part and a SUSY part,

$$\Delta r^{\rm NMSSM(h.o.)} = \Delta r^{\rm SM(h.o.)} + \Delta r^{\rm SUSY(h.o.)}. \tag{34}$$

The terms $\Delta r^{\rm SM/SUSY(h.o.)}$ describe the SM/SUSY contributions beyond one-loop order. For $\Delta r^{\rm SM(h.o.)}$ we employ the most up-to-date SM result including all relevant higher-order corrections, while $\Delta r^{\rm SUSY(h.o.)}$

contains the most up-to-date higher-order contributions of SUSY type (see below). The approach followed in Eq. (34) has several advantages. It ensures in particular that the best available SM prediction is recovered in the decoupling limit, where all superpartners are heavy, the singlet decouples, and the NMSSM Higgs sector becomes SM-like. Furthermore, the approach to combine the most up-to-date SM prediction with additional "new physics" contributions (here from supersymmetry) allows one to readily compare the MSSM and NMSSM predictions on an equal footing and it provides an appropriate framework also for an extension to other scenarios of physics beyond the SM.

The expression for the higher-order contributions given in Eq. (34) formally introduces a dependence of the NMSSM result on the SM Higgs mass, which enters from the two-loop electroweak corrections onwards. In those contributions we identify the SM Higgs mass with the mass of the NMSSM Higgs boson with the largest coupling to gauge bosons.

For the higher-order corrections in the SM, $\Delta r^{\rm SM(h.o.)}$, we incorporate the following contributions up to the four-loop order

$$\begin{aligned}\Delta r^{\rm SM(h.o.)} =& \Delta r^{(\alpha\alpha_s)} + \Delta r^{(\alpha\alpha_s^2)} + \Delta r^{(\alpha^2)}_{\rm ferm} + \Delta r^{(\alpha^2)}_{\rm bos} \\ &+ \Delta r^{(G_\mu^2\alpha_s m_t^4)} + \Delta r^{(G_\mu^3 m_t^6)} + \Delta r^{(G_\mu m_t^2 \alpha_s^3)} \,.\end{aligned} \tag{35}$$

The contributions in Eq. (35) consist of the two-loop QCD corrections $\Delta r^{(\alpha\alpha_s)}$ [35–40], the three-loop QCD corrections $\Delta r^{(\alpha\alpha_s^2)}$ [48–51], the fermionic electroweak two-loop corrections $\Delta r^{(\alpha^2)}_{\rm ferm}$ [42–44], the purely bosonic electroweak two-loop corrections $\Delta r^{(\alpha^2)}_{\rm bos}$ [45–47], the mixed QCD and electroweak three-loop contributions $\Delta r^{(G_\mu^2\alpha_s m_t^4)}$ [52,53], the purely electroweak three-loop contribution $\Delta r^{(G_\mu^3 m_t^6)}$ [52,53], and finally the four-loop QCD correction $\Delta r^{(G_\mu m_t^2\alpha_s^3)}$ [55–57].

The radiative corrections in the SM beyond one-loop level are numerically significant and lead to a large downward shift in M_W by more than 100 MeV.[5] The largest shift (beyond one-loop) is caused by the two-loop QCD corrections [35–41] followed by the three-loop QCD corrections $\Delta r^{(\alpha\alpha_s^2)}$ [48–51].

Most of the higher-order contributions are known analytically (and we include them in this form), except for the full electroweak two-loop contributions in the SM which involve numerical integrations of the two-loop scalar integrals. These contributions are included in our calculation using a simple parametrization formula given in [59].[6] This fit formula gives a good approximation to the full result for a light SM Higgs (the agreement is better than 0.4 MeV for M_W) [59]. Using this parametrization directly for the SM prediction of $\Delta r^{(\alpha^2)}_{\rm ferm} + \Delta r^{(\alpha^2)}_{\rm bos}$ (rather than for the full SM prediction of M_W — an approach followed for the MSSM case in Ref. [73] and for the NMSSM case in Ref. [78]) allows us to evaluate these contributions at the particular NMSSM value for M_W in each iteration step. The output of this formula approximates the full result of $\Delta r^{(\alpha^2)}_{\rm ferm} + \Delta r^{(\alpha^2)}_{\rm bos}$ using the fixed-width definition, such that it can directly be combined with other terms of our calculation.[7] In our expression for $\Delta r^{\rm SM(h.o.)}$ we use the result for $\Delta r^{(\alpha\alpha_s)}$ given in Ref. [37], which contains also contributions from quarks of the first two generations and is numerically very close to the result from Ref. [41],[8] and the result for

[5] The corrections beyond one-loop order are in fact crucial for the important result that the M_W prediction in the SM favours a light Higgs boson, whereas the one-loop result alone would favour a heavy SM Higgs.

[6] In [59] the electroweak two-loop contributions are expressed via $\Delta r^{(\alpha^2)} \equiv \Delta r^{(\alpha^2)}_{\rm ferm} + \Delta r^{(\alpha^2)}_{\rm bos} = (\Delta\alpha)^2 + 2\Delta\alpha\,\Delta\tilde{r}^{(\alpha)} + \Delta r^{(\alpha^2)}_{\rm rem}$, where a simple fit formula for the remainder term $\Delta r^{(\alpha^2)}_{\rm rem}$ is given. The quantity $\Delta\tilde{r}^{(\alpha)}$ in the second term denotes the full one-loop result without the $\Delta\alpha$ term.

[7] It should be noted, however, that the gauge boson masses with running width definition are needed as input for the fit formula given in [59]. This is the only part of our calculation where the running width definition is used internally.

[8] This is an improvement compared to Ref. [61], where the two-loop QCD contributions from Ref. [50] were employed, which include only the top und bottom quark contributions.

$\Delta r^{(\alpha\alpha_s^2)}$ from Ref. [50]. Both contributions are parametrized in terms of G_μ. A comparison between our evaluation of $M_W^{\rm SM}$ and the fit formula for $M_W^{\rm SM}$ given in Ref. [58] can be found in Sect. 4.3 below.

For the higher-order corrections of SUSY type, see Eq. (34), we take the following contributions into account,

$$\Delta r^{\rm SUSY(h.o.)} = \Delta r_{\rm red}^{\rm SUSY(\alpha^2)} - \frac{c_{\rm w}^2}{s_{\rm w}^2}\Delta\rho^{\rm SUSY,(\alpha\alpha_s)} - \frac{c_{\rm w}^2}{s_{\rm w}^2}\Delta\rho^{\rm SUSY,(\alpha_t^2,\alpha_t\alpha_b,\alpha_b^2)}\,, \tag{36}$$

incorporating all SUSY corrections beyond one-loop order that are known to date. The first term in Eq. (36) denotes the leading reducible $\mathcal{O}(\alpha^2)$ two-loop corrections. Those contributions are obtained by expanding the resummation formula [103]

$$1 + \Delta r = \frac{1}{(1-\Delta\alpha)\left(1+\frac{c_{\rm w}^2}{s_{\rm w}^2}\Delta\rho\right) - \Delta r_{\rm rem}}\,, \tag{37}$$

which correctly takes terms of the type $(\Delta\alpha)^2$, $(\Delta\rho)^2$ and $\Delta\alpha\Delta\rho$ into account[9] if $\Delta\rho$ is parametrized by G_μ. The pure SM terms are already included in $\Delta r^{\rm SM(h.o.)}$, and because of numerical compensations those contributions are small beyond two-loop order [41]. Thus, we only need to consider the leading two-loop terms with SUSY contributions,

$$\Delta r_{\rm red}^{\rm SUSY(\alpha^2)} = -\frac{c_{\rm w}^2}{s_{\rm w}^2}\Delta\alpha\Delta\rho^{\rm SUSY} + \frac{c_{\rm w}^4}{s_{\rm w}^4}(\Delta\rho^{\rm SUSY})^2 + 2\frac{c_{\rm w}^4}{s_{\rm w}^4}\Delta\rho^{\rm SUSY}\Delta\rho^{\rm SM}. \tag{38}$$

The other two terms in Eq. (36) denote irreducible two-loop SUSY contributions. The two-loop $\mathcal{O}(\alpha\alpha_s)$ SUSY contributions [74, 75], $\Delta\rho^{\rm SUSY,(\alpha\alpha_s)}$, contain squark loops with gluon exchange and quark/squark loops with gluino exchange (both depicted in Fig. 8). While the formula for the gluino contributions is very lengthy, a compact result exists for the gluon contributions to $\Delta\rho$ [74, 75]. Using these two-loop results for the SUSY contributions to M_W requires the on-shell (physical) values for the squark masses as input. The $SU(2)$ relation $M_{\tilde{t}_L} = M_{\tilde{b}_L}$ implies that one of the stop/sbottom masses is not independent, but can be expressed in terms of the other parameters. Therefore, when including higher-order contributions, one cannot choose independent renormalization conditions for all four (stop and sbottom) masses. Loop corrections to the relation between the squark masses must be taken into account in order to be able to insert the proper on-shell values for the squark masses into our calculation. This one-loop correction to the relation between the squark masses is relevant when inserted into the one-loop SUSY contributions to M_W, while it is of higher order for the two-loop SUSY contributions. In our evaluation of M_W this is taken into account by a "mass-shift" correction term. For more details see Ref. [75]. The gluon, gluino and mass-shift corrections, which are identical in the MSSM and the NMSSM, are included in our NMSSM result for M_W.

The third term in Eq. (36) denotes the dominant Yukawa-enhanced electroweak two-loop corrections to $\Delta\rho$ of $\mathcal{O}(\alpha_t^2)$, $\mathcal{O}(\alpha_t\alpha_b)$ and $\mathcal{O}(\alpha_b^2)$ [76, 77]. These contributions consist of heavy quark (t/b) loops with Higgs exchange, squark $(\tilde{t}/\tilde{b})$ loops with Higgs exchange, and mixed quark-squark loops with Higgsino exchange, see Fig. 9. The corrections of this kind, which depend on the specific form of the Higgs sector, are only known for the MSSM so far [76, 77]. It is nevertheless possible to take them into account also for the NMSSM in an approximate form. To this end, the considered NMSSM parameter point needs to be related to appropriate parameter values of the MSSM. Besides the values for $\tan\beta$, the sfermion trilinear couplings A_f, and all the soft mass parameters, which can be directly

[9] In principle one could also include the term $\Delta\alpha\Delta r_{\rm rem}$, which however is numerically small.

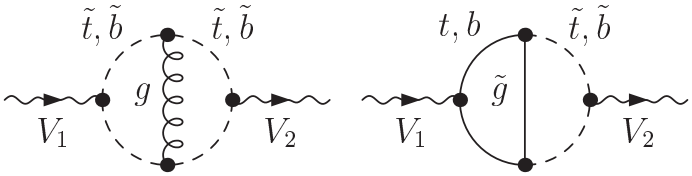

Figure 8: Generic $\mathcal{O}(\alpha\alpha_s)$ two-loop self-energy diagrams in the (N)MSSM. Here g denotes a gluon and $\tilde{g}$ a gluino; V_1,$V_2 = \gamma$,Z,$W^\pm$.

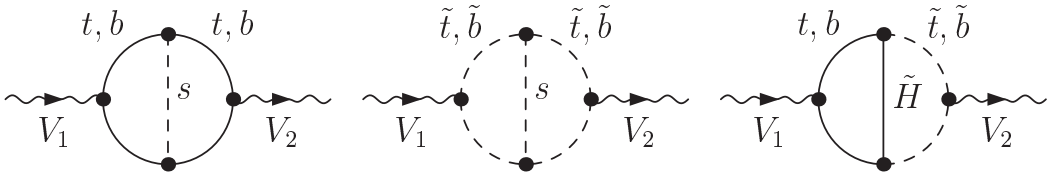

Figure 9: Generic $\mathcal{O}(\alpha_t^2 + \alpha_t\alpha_b + \alpha_b^2)$ two-loop diagrams, where $\tilde{H}$ denotes a Higgsino and is s either an NMSSM Higgs or a Goldstone boson; V_1,$V_2 = \gamma$,Z,$W^\pm$.

taken over from the parameter point in the NMSSM, we determine the parameters in the following way: we set the MSSM μ parameter equal to $\mu_{\rm eff}$ and we use the physical value of the charged Higgs mass as calculated in the NMSSM (see below) as input for the calculation of the MSSM Higgs masses. This prescription is motivated by the fact that in this way the value of the mass of the charged Higgs boson, which is the only Higgs boson appearing without mixing in both models, is the same in the NMSSM and the MSSM. The MSSM Higgs masses are calculated with `FeynHiggs` [104–108], using the calculated physical mass value of $M_{H^\pm}$ as on-shell input parameter. The MSSM Higgs masses and the Higgsino parameter μ determined in this way are then used as input for the calculation of $\Delta\rho$ to $\mathcal{O}(\alpha_t^2)$, $\mathcal{O}(\alpha_t\alpha_b)$, $\mathcal{O}(\alpha_b^2)$. In order to avoid double-counting the dominant Yukawa-enhanced electroweak two-loop corrections in the SM [109,110] have been subtracted according to Eq. (34). We find that the impact of the Yukawa-enhanced electroweak corrections of SUSY type on M_W is relatively small (typically $\lesssim 1$ MeV), and their numerical evaluation is rather time-consuming. In our numerical code for M_W in the NMSSM, we therefore leave it as an option to choose whether these contributions should be included or not. For the results presented in Sect. 4.4 they have not been included, unless stated otherwise.

4 Numerical results

4.1 Framework for the numerical analysis

For the evaluation of the W boson mass prediction, the masses of the NMSSM particles are needed. We use the NMSSM on-shell parameters as input to calculate the sfermion, chargino and neutralino masses. For the calculation of the Higgs boson masses we use `NMSSMTools` (version 4.6.0) [111–114].[10] For other tools that are available to calculate the NMSSM Higgs masses including higher-order radiative corrections see Refs. [115–117]. The implementation of the Higgs mass results of Ref. [117] (using directly the on-shell parameters as input) is in progress.

[10] In two plots below the NMSSM Higgs boson masses at tree-level are used. They are calculated using the tree-level relations given in Sect. 2.

In NMSSMTools the input parameters are assumed to be $\overline{\rm DR}$ parameters at the SUSY breaking scale. In order to use the NMSSMTools Higgs masses in our result, a transformation from the on-shell parameters, needed for our evaluation, to the $\overline{\rm DR}$ parameters, needed as NMSSMTools input, is necessary. This effect is approximately taken into account by transforming the on-shell X_t parameter into its $\overline{\rm DR}$ value by the relation given in Ref. [118] (equations (60) ff in Ref. [118]). The shift in the other parameters is significantly smaller and therefore neglected here.

We use a setup where the NMSSM parameter space can be tested against a broad set of experimental and theoretical constraints. Besides the constraints already implemented in NMSSMTools,[11] further direct constraints on the Higgs sectors are evaluated using the code HiggsBounds (version 4.2.0) [120–123]. All programs used for the numerical evaluation are linked through an interface to the NMSSM Mathematica code for the W boson mass prediction.[12]

4.2 Theoretical uncertainties

Before moving on to our numerical results for the W boson mass prediction in the NMSSM, we discuss the remaining theoretical uncertainties in the M_W calculation.

The dominant theoretical uncertainty of the prediction for M_W arises from the parametric uncertainty induced by the experimental error of the top-quark mass. Here one needs to take into account both the experimental error of the actual measurement and the systematic uncertainty associated with relating the experimentally determined quantity to a theoretically well-defined mass parameter, see the discussion above. A total experimental error of 1 GeV on m_t causes a parametric uncertainty on M_W of about 6 MeV, while the parametric uncertainties induced by the current experimental error of the hadronic contribution to the shift in the fine-structure constant, $\Delta\alpha_{\rm had}$, and by the experimental error of M_Z amount to about 2 MeV and 2.5 MeV, respectively. The uncertainty of the SM M_W prediction caused by the experimental error of the Higgs boson mass, $\delta M_H^{\rm exp} = 0.24$ GeV [60], is significantly smaller ($\lesssim 0.2$ MeV). In Ref. [32] the impact of improved accuracies of m_t and $\Delta\alpha_{\rm had}$ has been discussed. With a precise top mass measurement of $\Delta m_t = 0.1$ GeV (anticipated ILC precision) the associated parametric uncertainty in M_W is about 0.6 MeV.

The uncertainties from unknown higher-order corrections have been estimated to be around 4 MeV in the SM for a light Higgs boson ($M_{H^{\rm SM}} < 300$ GeV) [58]. The prediction for M_W in the NMSSM is affected by additional theoretical uncertainties from unknown higher-order corrections of SUSY type. While in the decoupling limit those additional uncertainties vanish, they can be important if some SUSY particles, in particular in the scalar top and bottom sectors, are relatively light. The combined theoretical uncertainty from unknown higher-order corrections of SM- and SUSY-type has been estimated (for the MSSM with real parameters) in Refs. [73, 77] as $\delta M_W \sim (4-9)$ MeV, depending on the SUSY mass scale.[13] Since we include the same SUSY higher-order corrections in our NMSSM calculation as were considered for the uncertainty estimate in the MSSM, the uncertainty from unknown

[11] NMSSMTools contains a number of theoretical and experimental constraints, e.g. constraints from collider experiments (such as LEP mass limits on SUSY particles), B-physics and astrophysics. More details on the constraints included in NMSSMTools can be found in Refs. [111, 119].

[12] The Mathematica code is linked to a Fortran driver program, calling NMSSMTools and HiggsBounds. The calculation of the SUSY particle masses is also included in the Fortran driver. Similarly to the MSSM case [61], we plan to additionally implement the M_W calculation directly into Fortran in order to increase the speed of the M_W evaluation. This will be useful in particular for large scans of the parameter space.

[13] The lower limit of 4 MeV corresponds to the SM uncertainty, which applies to the decoupling limit of the MSSM. For the upper limit of 9 MeV very light SUSY particles were considered. In view of the latest experimental bounds from the SUSY searches at the LHC, the (maximal) uncertainty from missing higher orders is expected to be somewhat smaller than 9 MeV.

$\Delta r^{(\alpha)}$	$\Delta r^{(\alpha\alpha_s)}$	$\Delta r^{(\alpha\alpha_s^2)}$	$\Delta r^{(\alpha^2)}_{\rm ferm} + \Delta r^{(\alpha^2)}_{\rm bos}$	$\Delta r^{(G_\mu^2\alpha_s m_t^4)} + \Delta r^{(G_\mu^3 m_t^6)}$	$\Delta r^{(G_\mu m_t^2 \alpha_s^3)}$
297.17	36.28	7.03	29.14	-1.60	1.23

Table 1: The numerical values ($\times 10^4$) of the different contributions to Δr specified in Eq. (35) are given for $M_W = 80.385$ GeV and $M_H^{\rm SM} = 125.09$ GeV.

higher-order corrections is estimated to be of similar size.

4.3 SM higher-order corrections

We compare our evaluation of $M_W^{\rm SM}$ to the result from the fit formula for $M_W^{\rm SM}$ given in Ref. [58]. In the latest version of Ref. [58] all the corrections of Eq. (35) are included. The M_W fit formula incorporates the $\mathcal{O}(\alpha\alpha_s)$ from Ref. [41], whereas we use the $\mathcal{O}(\alpha\alpha_s)$ from Ref. [37]. These results are in good numerical agreement with each other if in both cases the electric charge is parametrized in terms of the fine structure constant α. The $\mathcal{O}(\alpha^2\alpha_s)$ three-loop corrections included in Eq. (35) are parametrized in terms of G_μ. We therefore choose to parametrize the $\mathcal{O}(\alpha\alpha_s)$ contributions also in terms of G_μ. The difference between the G_μ parametrization of the QCD two-loop corrections that we use here and the α parametrization used in Ref. [58] leads to a prediction for $M_W^{\rm SM}$ that is ~ 2 MeV lower than the result given in Ref. [58].

The numerical values of the different SM-type contributions to Δr are given in table 1 for $M_W = 80.385$ GeV and $M_H^{\rm SM} = 125.09$ GeV. The other relevant input parameters that we use are

$$
\begin{aligned}
&m_t = 173.34 \text{ GeV}, \quad m_b = 4.7 \text{ GeV}, \quad M_Z = 91.1876 \text{ GeV}, \quad \Gamma_{\rm Z} = 2.4952 \text{ GeV},\\
&\Delta\alpha_{\rm lept} = 0.031497686, \quad \Delta\alpha^{(5)}_{\rm had} = 0.02757, \quad \alpha^{-1} = 137.035999074,\\
&\alpha_s(M_Z) = 0.1184, \quad G_\mu = 1.1663787 \times 10^{-5} \text{ GeV}^{-2}.
\end{aligned}
\tag{39}
$$

As explained above, the values for the W and Z boson masses given above, which correspond to a Breit-Wigner shape with running width, have been transformed internally to the definition of a Breit-Wigner shape with fixed width associated with the real part of the complex pole.

4.4 Results for the M_W prediction in the NMSSM

We now turn to the discussion of the prediction for M_W in the NMSSM. Our evaluation has been carried out for the case of real parameters, consequently for all parameters given in this section the phases are set to zero and will not be listed as separate input parameters.

An earlier result for M_W in the NMSSM was presented in Ref. [78]. Concerning SUSY two-loop contributions, in this result only the part of the contributions to $\Delta\rho^{\rm SUSY,(\alpha\alpha_s)}$, see Eq. (36), arising from squark loops with gluon exchange is taken into account. As we will show below in the discussion of our improved result for M_W in the NMSSM, the two-loop contributions that have been neglected in Ref. [78] can have a sizeable impact. A further improvement of our results for the MSSM and the NMSSM is that they are based on contributions to Δr that can all be evaluated at the correct input value for M_W (using an iterative procedure), i.e. $M_W^{\rm (N)MSSM}$, while the evaluation in Ref. [78] makes use of the fitting formula for $M_W^{\rm SM}$ [58]. The corresponding contribution to Δr extracted from the fitting formula for $M_W^{\rm SM}$ is determined at the input value $M_W^{\rm SM}$ rather than $M_W^{\rm (N)MSSM}$, while it is the latter that is actually needed for the evaluation in the (N)MSSM (see Ref. [73] for a discussion how to

remedy this effect). We have compared our result with the one given in Ref. [78][14] taking into account only those contributions in our result that are also contained in the result of Ref. [78]. We found good agreement in this case, at the level of 1–2 MeV on M_W.

Throughout this section, we only display parameter points that are allowed by the LEP limits on SUSY particle masses [124], by all theoretical constraints in `NMSSMTools` (checking e.g. that the Higgs potential has a viable physical minimum and that no Landau pole exists below the GUT scale), and have the neutralino as LSP. Unless stated otherwise, we choose the masses of the first and second generation squarks and the gluino to be large enough to not be in conflict with the limits from the searches for these particles at the LHC.[15] We make use of the code `HiggsBounds` [121–123] to check each parameter point against the limits from the Higgs searches at LEP, the Tevatron and the LHC.

4.4.1 Results in the MSSM limit of the NMSSM

Before turning to the discussion of the genuine NMSSM effects, we show the NMSSM M_W prediction in the MSSM limit

$$\lambda \to 0,\ \kappa \to 0, \qquad K \equiv \kappa/\lambda = \text{constant}, \tag{40}$$

with all other parameters (including μ_{eff}) held fixed (such that the MSSM is recovered). In this limit one $\mathcal{CP}$-even, one $\mathcal{CP}$-odd Higgs boson (not necessarily the heaviest ones) and one neutralino become completely singlet and decouple. In the discussion of M_W^{NMSSM} in the MSSM limit, the setup for the numerical evaluation is introduced and the comparison to the MSSM M_W prediction serves as validation of our implementation.

The left plot of Fig. 10 shows the NMSSM predictions in the MSSM limit (blue curves) as well as the MSSM predictions (red curves) for M_W as a function of the stop mixing parameter X_t.[16] The parameters in Fig. 10 are $m_t = 173.34$ GeV, $\tan\beta = 20$, $\mu_{(\text{eff})} = 200$ GeV, $M_{\tilde{L}/\tilde{E}} = 500$ GeV, $M_{\tilde{Q}/\tilde{U}/\tilde{D}_{1,2}} = 1500$ GeV, $M_{\text{SUSY}} = M_{\tilde{Q}_3} = M_{\tilde{U}_3} = M_{\tilde{D}_3} = 1000$ GeV, $A_\tau = A_b = A_t$, $M_2 = 200$ GeV and $m_{\tilde{g}} = 1500$ GeV. For the additional NMSSM parameters we choose $\hat{m}_A = 1000$ GeV, $\lambda \to 0$, $K = \kappa/\lambda = 0.5$, $A_\kappa = -100$ GeV (the impact of A_κ on M_W in the MSSM limit is negligible). Here, and in the following the prediction for M_W includes all higher-order corrections described above (besides the Higgsino two-loop corrections).

Our approach here is the following: We start from a NMSSM parameter point. We take the effective $\mathcal{CP}$-odd doublet mass $\hat{m}_A$ or the parameter A_λ (here $\hat{m}_A = 1000$ GeV) as input to calculate the NMSSM Higgs boson spectrum. The physical value of the charged Higgs mass (calculated in the NMSSM) is used as input for the calculation of the MSSM Higgs masses. As discussed in Sect. 3.3, this procedure ensures that the mass of the charged Higgs boson used in our M_W calculation is the same in the NMSSM and the MSSM, since we calculate the MSSM Higgs masses in `FeynHiggs` (version 2.10.4) where the input parameter $M_{H^\pm}$ is interpreted as an on-shell mass parameter. The other parameters which occur in both models ($\tan\beta$, the sfermion trilinear couplings A_f, and the soft mass parameters)

[14] We thank the authors of Ref. [78] for providing us with numerical results from their code.

[15] The most stringent limits from SUSY searches at the LHC are set on the masses of the first and second generation squarks and the gluino, which go beyond ~ 1 TeV. However these limits depend on the model assumptions. Relaxing these assumptions, squarks can still be significantly lighter [125]. Substantially weaker limits have been reported for the particles of the other sectors, so that third-generation squarks, stops and sbottoms, as well as the uncoloured SUSY particles, are significantly less constrained by LHC searches.

[16] The X_t parameter that we plot here is the on-shell parameter. As described in Sect. 4.1 the on-shell value is transformed into a $\overline{\text{DR}}$ value, which is used as input for `NMSSMTools` to calculate the Higgs masses. All numerical values given for X_t in this section refer to the on-shell parameters.

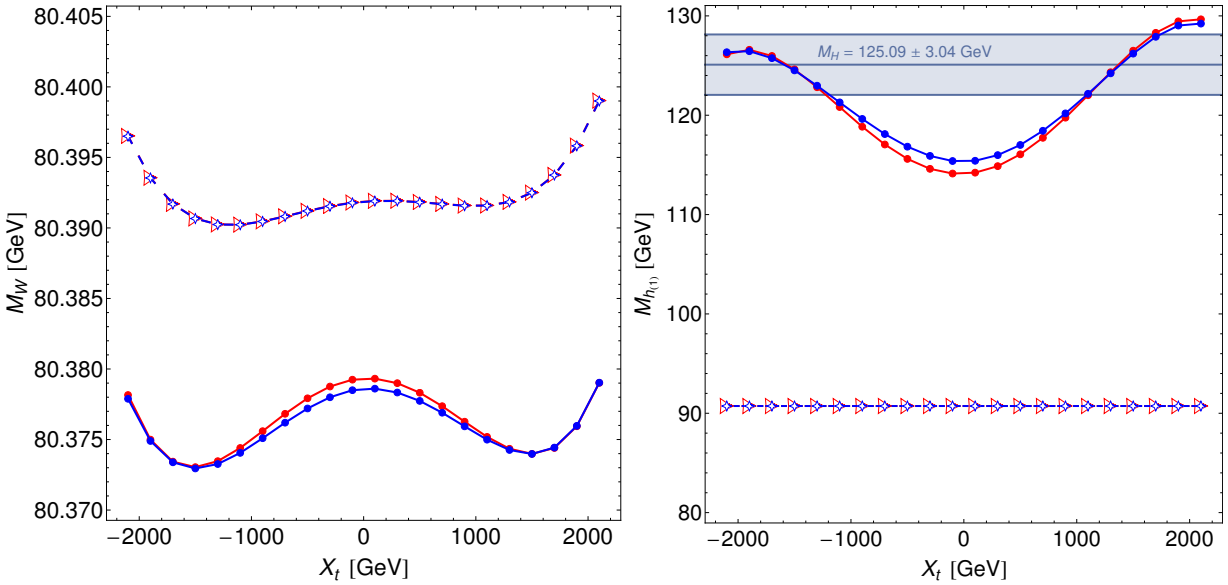

Figure 10: Comparison of the NMSSM predictions in the MSSM limit (blue curves) for the W boson mass (left plot) and the lightest $\mathcal{CP}$-even Higgs mass (right plot) with the MSSM predictions (red curves) plotted against the stop mixing parameter X_t. The parameters are given in the text. For the two dashed curves (small blue diamonds for the NMSSM predictions in the MSSM limit, and red triangles for the MSSM predictions) the tree-level Higgs masses are used. For the solid curves (with filled dots) loop-corrected Higgs masses are used: the NMSSM Higgs masses are calculated with `NMSSMTools`, and the MSSM Higgs masses calculated with `FeynHiggs`.

are used with the same values as input for the calculation of the physical masses in the MSSM and the NMSSM. For the Higgs mass calculation with `NMSSMTools` the parameter X_t is transformed into a $\overline{\rm DR}$ parameter, while for the $M_W^{\rm (N)MSSM}$ calculations its on-shell value is used. The MSSM parameter μ is identified with the NMSSM effective value $\mu_{\rm eff}$.[17]

For the two dashed curves in Fig. 10 (small blue diamonds for the NMSSM predictions in the MSSM limit and red open triangles for the MSSM predictions) the tree-level Higgs masses are used. For the solid curve (with filled dots) loop-corrected Higgs masses are used: the NMSSM Higgs masses are calculated with `NMSSMTools` and the MSSM Higgs masses calculated with `FeynHiggs`.

The corresponding predictions for the lightest $\mathcal{CP}$-even Higgs mass in the (N)MSSM are displayed in the right plot of Fig. 10. For illustration, in the plots for the Higgs mass predictions the theoretical uncertainty on the SUSY Higgs mass is combined with the experimental error into an allowed region for the Higgs boson mass, rather than displaying the theoretical uncertainty in the Higgs mass prediction as a band around the theory prediction. Consequently, the blue band in the right plot shows the region $M_H = 125.09 \pm 3.04$ GeV, which was obtained by adding a theoretical uncertainty of 3 GeV quadratically to the experimental 2σ error. Here M_H represents the corresponding mass parameter in the MSSM and the NMSSM (in the considered case M_h in the MSSM and M_{h_1} in the NMSSM). The position of the curves relative to the blue M_H band depends strongly on the other parameters, which are fixed here. The range in which the NMSSM parameter points (with `NMSSMTools` Higgs masses) are allowed by `HiggsBounds` coincides (approximately) with the region in with the lightest

[17] From here on we will leave out the subscript 'eff' for the μ parameter in the NMSSM

Higgs mass is heavy enough to be interpreted as the signal at 125.09 GeV ($|X_t| \gtrsim 1000$ GeV and $X_t < 1900$ GeV). While the tree-level Higgs masses agree exactly in the MSSM and the NMSSM in the MSSM limit, we observe a small difference between the masses for the lightest $\mathcal{CP}$-even Higgs calculated with `FeynHiggs` and with `NMSSMTools`. This discrepancy arises because of differences in the higher-order corrections implemented in the two codes[18]. The tree-level Higgs masses are only used in Fig. 10 for illustration. In all following plots (if nothing else is specified) the full loop-corrected results for the Higgs masses are used.

Going back to the left plot of Fig. 10, we see that the $M_W^{\rm NMSSM}$ predictions in the MSSM limit and the $M_W^{\rm MSSM}$ prediction coincide exactly if tree-level Higgs masses are used (which is an important check of our implementation). However, using loop-corrected masses, the difference between the `FeynHiggs` and `NMSSMTools` predictions for the lightest $\mathcal{CP}$-even Higgs mass leads to a difference in M_W of ~ 0.8 MeV for small $|X_t|$. The effect of the difference in the M_W prediction induced by the different Higgs mass predictions is contained in the following plots in this section. This should be kept in mind when comparing $M_W^{\rm NMSSM}$ with $M_W^{\rm MSSM}$.

The dependence of the M_W predictions in Fig. 10 on X_t is influenced both by the loop contributions to Δr involving stops and sbottoms, which are identical at the one-loop level in the MSSM and the NMSSM, and indirectly via the behaviour of the lightest $\mathcal{CP}$-even Higgs mass. In the chosen example the impact of the former contributions is relatively small as a consequence of the relatively high mass scale in the stop and sbottom sector. The effect of the higher-order corrections in the Higgs sector is clearly visible in Fig. 10 by comparing the full predictions with the ones based on the tree-level Higgs masses. As expected from the behaviour of the M_W prediction in the SM on the Higgs boson mass, the upward shift in the mass of the lightest $\mathcal{CP}$-even Higgs boson caused by the loop corrections gives rise to a sizeable downward shift in the predictions for M_W. The local maximum in the M_W predictions at about $X_t = 0$ is in accordance with the local minimum in the Higgs-mass predictions. The fact that the local minima in the M_W predictions are somewhat shifted compared to the local maxima in the Higgs-mass predictions is caused by the stop-loop contributions to Δr, whose effect can be directly seen for the curves based on the tree-level predictions for the mass of the lightest $\mathcal{CP}$-even Higgs boson in the left plot of Fig. 10. The main contribution of the stop/sbottom sector can be associated with $\Delta\rho$ and hence depends strongly on the squark mixing. $\Delta\rho$ contains terms sensitive to the splitting between the squarks of one flavour and terms sensitive to the splitting between stops and sbottoms. These two contributions enter with opposite signs, which tend to compensate each other for small and moderate values of X_t.

4.4.2 SUSY higher-oder corrections

Now we turn to the discussion of the size and parameter dependence of the SUSY two-loop corrections. Fig. 11 shows the size of the $\mathcal{O}(\alpha\alpha_s)$ two-loop corrections. The parameters used here are $m_t = 173.34$ GeV, $\tan\beta = 2$, $\mu = 200$ GeV, $M_{\tilde{L}/\tilde{E}} = 1000$ GeV, $M_{\tilde{Q}/\tilde{U}/\tilde{D}_{1,2}} = 1500$ GeV, $A_\tau = A_b =$

[18] In `NMSSMTools` the user can set a flag determining the precision for the Higgs masses. The result from Ref. [126] containing contributions up to the two-loop level is used if the flag is set equal to 1 or 2, where the two flags correspond to the result without (flag 1) and including (flag 2) contributions from non-zero momenta in the one-loop self-energies. While in `FeynHiggs` this momentum dependence is taken into account, we nevertheless find better numerical agreement with flag 1 of the `NMSSMTools` result. For the sake of comparison between the NMSSM and the MSSM predictions for M_W it is useful to keep those differences arising from different higher-order corrections in the MSSM limit of the Higgs sector as small as possible. We have therefore chosen flag 1 for the Higgs-mass evaluation with `NMSSMTools` in our numerical analyses presented in this paper. As mentioned above, an implementation of our predictions using the Higgs-mass evaluation of Ref. [117] is in progress.

1000 GeV, $M_2 = 600$ GeV, $m_{\tilde{g}} = 1500$ GeV (solid curves) and $m_{\tilde{g}} = 300$ GeV (dashed curves), $A_\lambda = 395$ GeV, $\lambda = 0.57$, $\kappa = 0.2$, $A_\kappa = -80$ GeV and we vary $M_{\rm SUSY} = M_{\tilde{Q}_3} = M_{\tilde{U}_3} = M_{\tilde{D}_3}$. We show the results for three values of X_t: $X_t = 2\,M_{\rm SUSY}$ (left), $X_t = 0$ (middle) and $X_t = -2\,M_{\rm SUSY}$ (right). It should be stressed here that the parameters for these plots are chosen to demonstrate the possible size and the parameter dependence of the SUSY two-loop corrections, however they are partially excluded by experimental data: The parameter points in the left plots with $X_t = 2\,M_{\rm SUSY}$ are `HiggsBounds` allowed for $M_{\rm SUSY} \lesssim 800$ GeV (apart from a small excluded island around $M_{\rm SUSY} \sim 550$ GeV), whereas in the middle and the right plots, the chosen parameters are `HiggsBounds` excluded for most $M_{\rm SUSY}$ values. A gluino mass value of $m_{\tilde{g}} = 300$ GeV is clearly disfavoured by the negative LHC search results. Fig. 11 shows the contribution to the W boson mass, δM_W, from the $\mathcal{O}(\alpha\alpha_s)$ two-loop corrections with gluon exchange (dark blue curves), with gluino exchange (orange curves) and from the mass-shift correction (pink curves). The shift δM_W has been obtained by calculating $M_W^{\rm NMSSM}$ twice, once including the corresponding two-loop corrections, and once without, and the two results have been subtracted from each other. Starting with the dark blue curves, we find that the gluon contributions lead to a maximal shift of ~ 3 MeV in M_W for all three choices of X_t and that the size of the gluon contributions decreases with increasing $M_{\rm SUSY}$. Turning to the orange curves, we find that for $m_{\tilde{g}} = 1500$ GeV (solid curves) the δM_W shift, induced by the gluino two-loop corrections, is small (< 1 MeV) for $X_t = 0$, while it is up to $3 - 4$ MeV for $X_t = 2\,M_{\rm SUSY}$ and $X_t = -2\,M_{\rm SUSY}$. Making the gluino light — choosing $m_{\tilde{g}} = 300$ GeV (dashed curves) — the gluino corrections can get large. For large positive squark mixing, $X_t = 2\,M_{\rm SUSY}$, they reach up to 17 MeV for small values of $M_{\rm SUSY}$. The gluino corrections can lead to both a positive and a negative M_W shift, depending on the stop mixing parameter. Threshold effects occur in the gluino corrections and cause kinks in the orange curves, as can be seen in the middle and the right plots.

The gluon and gluino two-loop contributions are directly related to the mass-shift correction, which has to be incorporated in order to arrive at the complete result for the $\mathcal{O}(\alpha\alpha_s)$ contributions to $\Delta\rho^{\rm SUSY}$. The pink curves show the impact of this additional correction term. Starting with the solid curves ($m_{\tilde{g}} = 1500$ GeV), we observe that for large stop mixing, $X_t = \pm 2\,M_{\rm SUSY}$, the mass-shift corrections are positive and the maximal shift is ~ 4 MeV. For zero mixing the mass-shift corrections lead to a large negative shift in M_W (up to -12 MeV for small $M_{\rm SUSY}$). For $m_{\tilde{g}} = 300$ GeV, the size of the mass-shift correction is smaller. The kinks, caused by threshold effects, can be observed (for the same $M_{\rm SUSY}$ values) also in the mass-shift corrections. Adding up the gluino and mass-shift corrections leads to a smooth curve and no kink is found in the full M_W prediction. This can be seen in Fig. 12, where we plot the sum of the gluon, gluino and mass-shift corrections (all parameters are the same as in Fig. 11). Generally one can see that for large $M_{\rm SUSY}$ all contributions decrease, showing the expected decoupling behaviour. However contributions from the $\mathcal{O}(\alpha\alpha_s)$ two-loop corrections up to a few MeV are still possible for $M_{\rm SUSY} = 1000$ GeV.

The Yukawa-enhanced electroweak two-loop corrections of $\mathcal{O}(\alpha_t^2)$, $\mathcal{O}(\alpha_t\alpha_b)$, $\mathcal{O}(\alpha_b^2)$ to $\Delta\rho$ ("Higgsino corrections") in the MSSM can be included in our code, as discussed in Sect. 3.3. To do so, we calculate the MSSM Higgs masses as described in Sect. 3.3 (taking the NMSSM charged Higgs mass as input for the MSSM Higgs mass calculation) and use them as input for the $\Delta\rho$ ($\mathcal{O}(\alpha_t^2)$, $\mathcal{O}(\alpha_t\alpha_b)$, $\mathcal{O}(\alpha_b^2)$) formula. The size of these contributions can be seen in Fig. 13. Here, and in some of the following plots, we choose modified versions of the benchmark points given in Ref. [127], which predict one of the $\mathcal{CP}$-even NMSSM Higgs bosons in the mass range of the observed Higgs signal, as starting point for our study. Here we take the following parameters: $m_t = 173.34$ GeV, $\tan\beta = 2$, $\mu = 200$ GeV, $M_{\tilde{L}/\tilde{E}} = 1000$ GeV, $M_{\tilde{Q}/\tilde{U}/\tilde{D}_{1,2}} = 1200$ GeV, $M_{\tilde{Q}_3} = M_{\tilde{U}_3} = 700$ GeV, $M_{\tilde{D}_3} = 1000$ GeV, $A_\tau = A_b = 1000$ GeV, $M_2 = 200$ GeV, $m_{\tilde{g}} = 1500$ GeV, $A_\lambda = 405$ GeV, $\lambda = 0.6$,

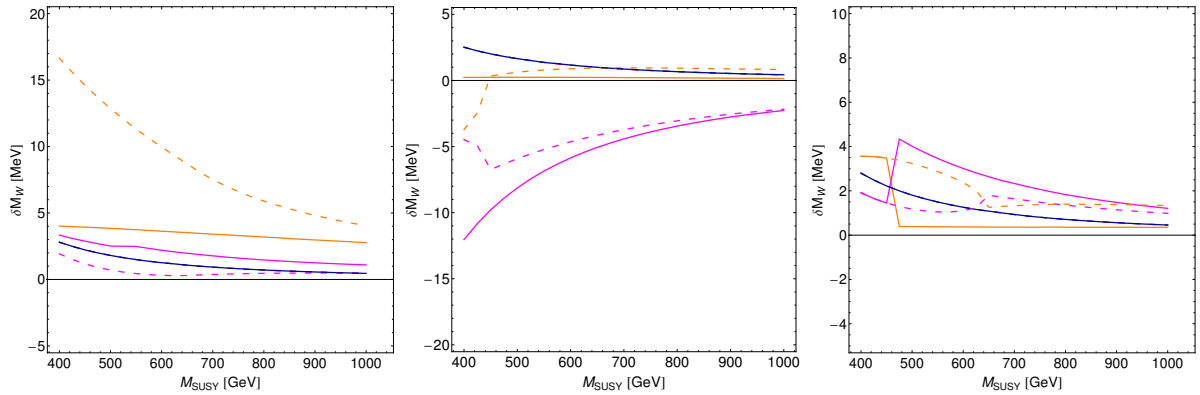

Figure 11: Size of the $\mathcal{O}(\alpha\alpha_s)$ two-loop corrections with gluon and gluino exchange. The solid curves correspond to $m_{\tilde{g}} = 1500$ GeV while the dashed curves correspond to $m_{\tilde{g}} = 300$ GeV. In the left plot we set $X_t = 2\,M_{\rm SUSY}$, in the middle one $X_t = 0$ and in the right one $X_t = -2\,M_{\rm SUSY}$. The plots show the contribution to the W boson mass, δM_W, from the $\mathcal{O}(\alpha\alpha_s)$ two-loop corrections with gluon exchange (dark blue curves), with gluino exchange (orange curves), and the mass-shift correction (pink curves) as a function of $M_{\rm SUSY}$. The parameter points with $X_t = 2\,M_{\rm SUSY}$ are `HiggsBounds` allowed for $M_{\rm SUSY} \lesssim 800$ GeV, whereas the points with $X_t = 0$ and with $X_t = -2\,M_{\rm SUSY}$ predict too low Higgs masses and are `HiggsBounds` excluded for most $M_{\rm SUSY}$ values. Note the different scales at the y-axis. The parameters used are given in the text.

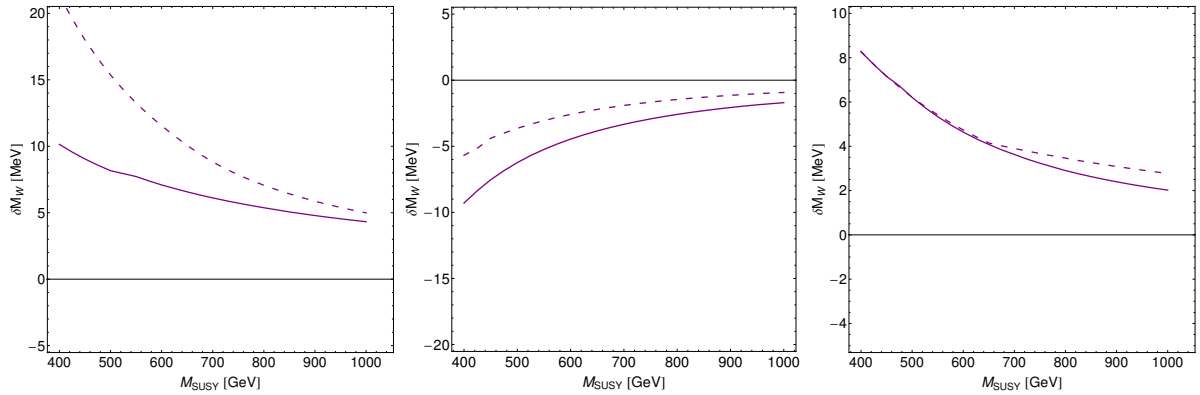

Figure 12: The plots show the full $\mathcal{O}(\alpha\alpha_s)$ two-loop corrections to M_W (sum of the corrections shown separately in Fig. 11) as a function of $M_{\rm SUSY}$. The parameters are the same as in Fig. 11. The solid curves correspond to $m_{\tilde{g}} = 1500$ GeV while the dashed curves correspond to $m_{\tilde{g}} = 300$ GeV. In the left plot we set $X_t = 2\,M_{\rm SUSY}$, in the middle one $X_t = 0$ and in the right one $X_t = -2\,M_{\rm SUSY}$.

$\kappa = 0.18$, $A_\kappa = -10$ GeV, and we vary X_t. These parameter points are `HiggsBounds` allowed in the regions 700 GeV $< X_t <$ 1000 GeV and 1100 GeV $< X_t <$ 1400 GeV. The left plot shows the NMSSM M_W prediction without Higgsino corrections (blue) and including Higgsino corrections (green) plotted against X_t. In the middle plot the shift δM_W induced by the Higgsino corrections (obtained by subtracting the M_W predictions with and without Higgsino corrections as shown in the left plot) is plotted against X_t. We see that the Higgsino corrections can enter the M_W prediction with both signs. The numerical effect of the M_W shift, induced by the Higgsino corrections, is relatively small

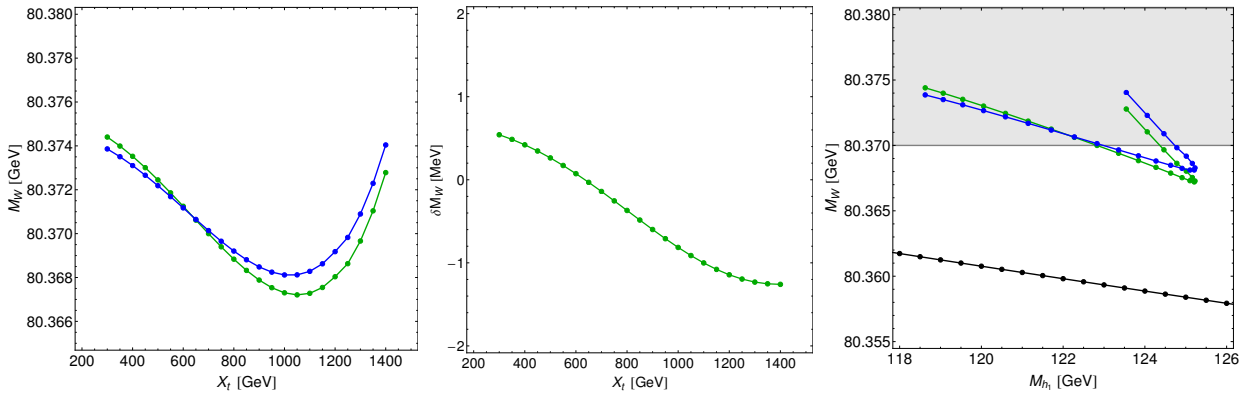

Figure 13: Size of the electroweak $\mathcal{O}(\alpha_t^2)$, $\mathcal{O}(\alpha_t\alpha_b)$, $\mathcal{O}(\alpha_b^2)$ SUSY two-loop corrections. The left plot shows the NMSSM M_W prediction without Higgsino corrections (blue) and including Higgsino corrections (green). The middle plot shows the shift δM_W induced by the Higgsino corrections (obtained by subtracting the M_W predictions with and without Higgsino corrections as shown in the left plot). The right plot shows the NMSSM M_W prediction without Higgsino corrections (blue) and including Higgsino corrections (green) plotted against the lightest $\mathcal{CP}$-even Higgs mass M_{h_1}. The black curve in the right plot indicates the SM M_W prediction with $M_{H^{\rm SM}} = M_{h_1}$. The grey band indicates the $1\,\sigma$ region of the experimental W boson mass measurement. The parameters used for these plots are given in the text.

(~ 1 MeV). It was shown in Ref. [77] that the contributions to M_W from the Higgsino corrections can be slightly larger (~ 5 MeV) for lighter $\tilde{t}/\tilde{b}$. The right plot shows the M_W prediction plotted against M_{h_1}. We can clearly see here that this scenario, in which the Higgs signal can be interpreted as the lightest $\mathcal{CP}$-even NMSSM Higgs, gives a W boson mass prediction in good agreement with the M_W measurement indicated by the grey band.

4.4.3 NMSSM Higgs sector contributions

Now we turn to the discussion of effects from the NMSSM Higgs sector. In the MSSM the maximal value for the tree-level Higgs mass M_h is M_Z. One of the features of the NMSSM Higgs sector is that the tree-level Higgs mass M_{h_1} gets an additional contribution $\lambda^2 v^2 \sin^2 2\beta$, which can shift the tree-level Higgs mass upwards compared to its MSSM value (an upward shift can also be caused by singlet–doublet mixing, if the singlet state is lighter than the doublet state), and thus reduce the size of the radiative corrections needed to 'push' the lightest Higgs mass up to the experimental value. For $\lambda = 0.7$ and $\tan\beta = 2$ a tree-level value for M_{h_1} of 112 GeV is possible [127]. This additional tree-level contribution to the Higgs mass, as well as its impact on M_W are shown in Fig. 14. The parameters chosen here are $m_t = 173.34$ GeV, $\mu = 500$ GeV, $M_{\tilde{L}/\tilde{E}} = 500$ GeV, $M_{\tilde{Q}/\tilde{U}/\tilde{D}_{1,2}} = 1500$ GeV, $M_{\tilde{Q}_3} = M_{\tilde{U}_3} = M_{\tilde{D}_3} = 1000$ GeV, $X_t = 2000$ GeV, $A_\tau = A_b = A_t$, $M_2 = 200$ GeV, $m_{\tilde{g}} = 1500$ GeV, $\hat{m}_A = 450$ GeV, $\kappa = \lambda$ and $A_\kappa = -100$ GeV. We vary $\tan\beta$ and show the results for different values of λ. The red curves correspond to the MSSM limit ($\lambda \to 0$) while for the other curves the λ value is given in the corresponding colour. The upper left plot shows the tree-level prediction for the lightest $\mathcal{CP}$-even Higgs mass M_{h_1}. As expected, the M_{h_1} prediction in the MSSM limit approaches its maximal value M_Z for large $\tan\beta$. Increasing λ, the M_{h_1} prediction decreases for large $\tan\beta$, caused by doublet–singlet mixing terms. For small $\tan\beta$ one clearly sees the positive contribution from the

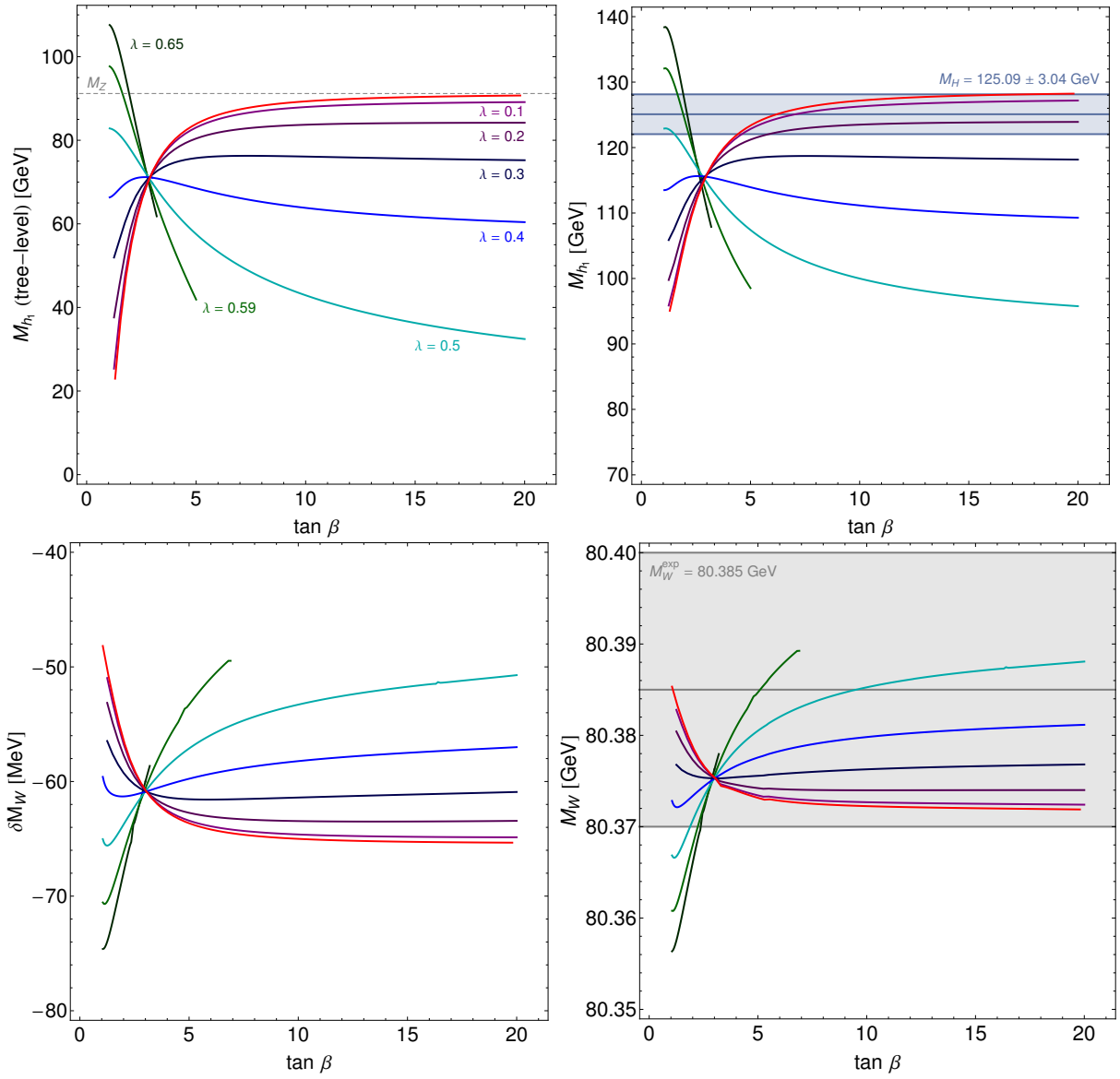

Figure 14: Predictions for M_{h_1} and M_W as a function of $\tan\beta$. The red curves correspond to the MSSM limit ($\lambda \to 0$) while for the other curves the λ values are given in the figure. The upper left plot shows the tree-level prediction for the lightest $\mathcal{CP}$-even Higgs mass M_{h_1}, the upper right plot shows M_{h_1} including radiative corrections (calculated with `NMSSMTools` as described in the text), the lower left plot shows the shift δM_W (calculated as in Eq. (41)) from diagrams involving Higgs and gauge bosons, and the lower right plot shows the full M_W prediction. The parameters used for these plots are given in the text.

term $\lambda^2 v^2 \sin^2 2\beta$ pushing the tree-level Higgs mass beyond M_Z for large λ.[19] The full M_{h_1} prediction

[19] The mixing of the h_1 state with the heavier singlet leads to a negative contribution to the tree-level Higgs mass, which pulls the NMSSM Higgs mass value down (compared to the MSSM case) for intermediate and large $\tan\beta$ values (for details see Ref. [4]). At a specific $\tan\beta$ value this contributions exactly cancels the positive $\lambda^2 v^2 \sin^2 2\beta$ shift at

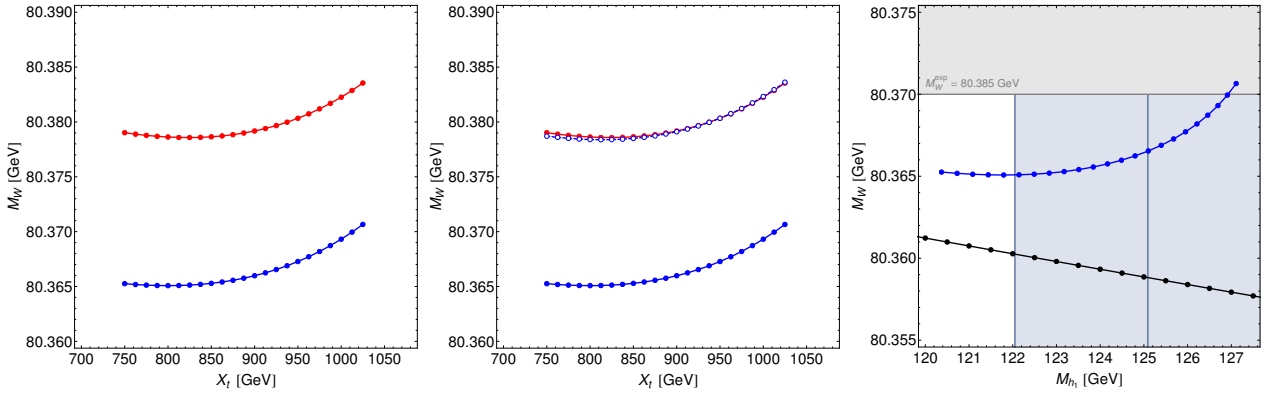

Figure 15: The left plot shows the $M_W^{\rm NMSSM}$ prediction (blue, solid curve) and the $M_W^{\rm MSSM}$ prediction (red) plotted against X_t. In the middle plot, the additional dashed blue curve corresponds to $M_W^{\rm NMSSM} - M_W^{\rm SM}(M_{h_1}) + M_W^{\rm SM}(M_h)$ (M_{h_1} is the mass of the lightest $\mathcal{CP}$-even Higgs of the NMSSM, and M_h is the mass of the light $\mathcal{CP}$-even Higgs of the MSSM). The right plots shows the $M_W^{\rm NMSSM}$ prediction plotted against the lightest $\mathcal{CP}$-even Higgs mass M_{h_1}. The black curve in the right plot indicates the SM M_W prediction with $M_{H^{\rm SM}} = M_{h_1}$. The experimental M_W measurement is indicated by the grey band; the region $M_H = 125.09 \pm 3.04$ GeV is indicated by the blue band. The parameters are given in the text.

(calculated with `NMSSMTools` as described above) can be seen in the upper right plot. Now we turn to the M_W contributions from the NMSSM Higgs and gauge boson sector, shown in the lower left plot. The shift δM_W displayed here is based on the approximate relation [73]

$$\delta M_W = -\frac{M_W^{\rm ref}}{2} \frac{s_W^2}{c_W^2 - s_W^2} \Delta r^{x(\alpha)}, \tag{41}$$

where $\Delta r^{x(\alpha)}$ denotes the one-loop contribution from particle sector x (here x=gauge-boson/Higgs), as defined for the NMSSM in Eq. (33). The reference M_W value is set here to $M_W^{\rm ref} = M_W^{\rm exp}$. The overall contribution from the Higgs sector is rather large and negative. As we will discuss in more detail below, the Higgs sector contributions here are predominantly SM-type contributions (with $M_{H^{\rm SM}}$ set to the corresponding Higgs mass value). The prediction for M_W in the NMSSM is shown in the lower right plot. Larger values for M_{h_1} correspond to a lower predicted value for M_W. Thus, for small $\tan\beta$, where we find a significantly higher predicted value for M_{h_1} for large λ than in the MSSM limit (arising from the additional tree-level term), we get a lower predicted value for M_W, which is however still compatible with the experimental M_W measurement at the 2σ level for the scenario chosen here. For $\tan\beta \sim 1$ the difference between the W boson mass prediction for $\lambda = 0.65$ and $\lambda \to 0$ is $\sim$ 25 MeV. The parameter $\tan\beta$ enters also in the sfermion and in the chargino/neutralino sector. We checked that for the parameters used here, the $\tan\beta$ dependence of the contributions from these two sectors is small compared to the Higgs sector contributions, less than ~ 3 MeV.

We continue the study of the NMSSM Higgs sector contributions in Fig. 15. In the left plot we compare the NMSSM prediction for M_W (blue curve) with the MSSM prediction (red curve).

the tree level, and the NMSSM Higgs mass value coincides with the MSSM value. In the scenario considered here, this happens for all λ at the same $\tan\beta$ value, since we chose $\kappa = \lambda$. As can be seen in the upper right plot of Fig. 14, this behaviour is approximately retained also in the presence of higher-order corrections in the Higgs sector.

The parameters we use here are $m_t = 173.34$ GeV, $\tan\beta = 2$, $\mu = 200$ GeV, $M_{\tilde{L}/\tilde{E}} = 1500$ GeV, $M_{\tilde{Q}/\tilde{U}/\tilde{D}_{1,2}} = 1200$ GeV, $M_{\tilde{U}_3} = M_{\tilde{Q}_3} = 540$ GeV, $M_{\tilde{D}_3} = 1000$ GeV, $A_\tau = A_b = 1000$ GeV, $M_2 = 370$ GeV, $m_{\tilde{g}} = 1500$ GeV, $A_\lambda = 420$ GeV, $\lambda = 0.57$, $\kappa = 0.2$, $A_\kappa = -10$ GeV, and we vary X_t. The NMSSM parameters are allowed by `HiggsBounds` for $X_t \gtrsim 780$ GeV. For $X_t \gtrsim 810$ GeV the mass of the lightest $\mathcal{CP}$-even Higgs falls in the range of the observed Higgs signal. The MSSM prediction is plotted as a comparison to illustrate and discuss the NMSSM effects on M_W. Here (and in the following) we do not check any phenomenological constraints for the MSSM parameter point (but only for the considered NMSSM scenario).

The NMSSM prediction for M_W differs from the MSSM prediction by ~ 12 MeV. The chargino/neutralino contributions can enter with both signs, and we find that in this scenario the relatively small μ value causes negative corrections to Δr. On the other hand, small M_2 values tend to give positive contributions to Δr. For the chosen parameters, these two effects cancel and contributions from the chargino/neutralino sector are very small, $\mathcal{O}(0.1$ MeV). Consequently, different Higgs sector contributions give rise to the difference between the MSSM and the NMSSM curves. Any differences in the $\mathcal{CP}$-odd Higgs sector have a negligible impact on the M_W prediction (see also Ref. [78]). Since we set the charged Higgs masses equal to each other in the two models, differences can only come from the $\mathcal{CP}$-even Higgs sector. For this parameter point the second lightest Higgs ($M_{h_2} = 150$ GeV) has a large singlet component ($|U_{23}^H|^2 \simeq 95\%$), consequently the singlet components of h_1 and h_3 are small. h_3 is heavy and has no impact on the M_W prediction. Our procedure to calculate the Higgs masses in the MSSM and the NMSSM leads to the same charged Higgs masses, but to different predictions for the lightest $\mathcal{CP}$-even Higgs masses M_{h_1} and M_h. This difference arises from the different relations between the charged Higgs mass and the lightest $\mathcal{CP}$-even Higgs mass in the MSSM and the NMSSM. Further it also incorporates the ("technical") difference due to the different radiative corrections included in `FeynHiggs` and `NMSSMTools` (as analysed above in the MSSM limit). The middle plot of Fig. 15 shows in addition to the NMSSM prediction for M_W (blue) and the MSSM prediction (red), a blue dashed curve (with open dots). The dashed blue curve corresponds to $M_W^{\rm NMSSM} - M_W^{\rm SM}(M_{h_1}) + M_W^{\rm SM}(M_h)$[20]. As one can see the dashed blue curve is very close to the red MSSM curve, thus here the difference between the MSSM and the NMSSM Higgs sector contributions to M_W essentially arises from the SM-type Higgs sector contributions, in which different Higgs mass values are inserted. It should be noted in this context that we have made a choice here by comparing the predictions for a particular NMSSM parameter point with an associated MSSM parameter point having the same value of the mass of the charged Higgs boson. Accordingly, the predictions for the other Higgs boson masses in the two models in general differ from each other, see above, leading to the effect displayed in the left plot of Fig. 15. Instead, one could have chosen, at least in principle, the associated MSSM parameter point such that the masses of the lightest $\mathcal{CP}$-even Higgs masses, M_{h_1} and M_h, are equal to each other. Also in that case differences in the other parameters in the Higgs sector, including the mass of the charged Higgs boson, would induce a shift in the predictions for M_W.

The right plot of Fig. 15 shows the $M_W^{\rm NMSSM}$ prediction plotted against the lightest $\mathcal{CP}$-even Higgs mass M_{h_1}. In this plot we display both the blue band indicating the region $M_{h_1} = 125.09 \pm 3.04$ GeV as well as the grey band showing the experimental $1\,\sigma$ band from the W boson mass measurement. The black curve in the right plot indicates the SM M_W prediction for $M_{H^{\rm SM}} = M_{h_1}$. It is interesting to note that in the NMSSM it is possible to find both the predictions for M_W and for the lightest $\mathcal{CP}$-even Higgs mass in the preferred regions indicated by the blue and grey bands in Fig. 15. For the

[20] The difference in the predictions for the lightest $\mathcal{CP}$-even Higgs masses in the MSSM and the NMSSM, which we subtract this way, includes both the difference between the different mass relations in the MSSM and the NMSSM, as well as the "technical" difference between the `FeynHiggs` and the `NMSSMTools` evaluation.

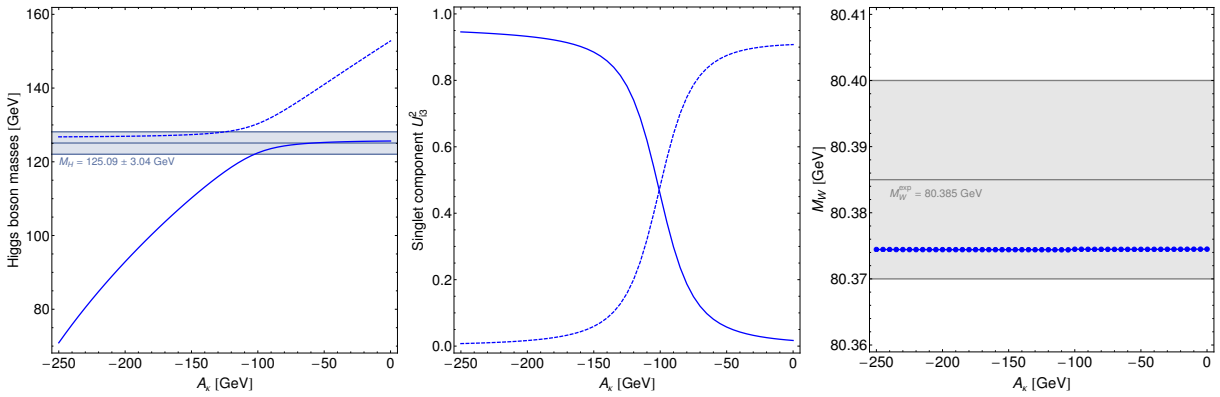

Figure 16: The left plot shows the prediction for M_{h_1} (solid curve) and M_{h_2} (dashed curve) as a function of A_κ. The region 125.09 ± 3.04 GeV is indicated as a blue band. The middle plot shows the singlet components of h_1 and h_2, U_{13}^2 (solid) and U_{23}^2 (dashed), respectively. The right plot shows the $M_W^{\rm NMSSM}$ prediction. Here the grey band shows the experimental $1\,\sigma$ band from the W boson mass measurement. The parameters used for these plots are given in the text.

SM, on the other hand, Fig. 15 shows the well-known result that setting the SM Higgs boson mass to the measured experimental value one finds a predicted value for M_W which is somewhat low compared to the experimental value.

Now we want to investigate whether singlet–doublet mixing (a genuine NMSSM feature) has a significant impact on the M_W prediction. Such a scenario is analysed in Fig. 16. Our parameters are $m_t = 173.34$ GeV, $\tan\beta = 2$, $\mu = 140$ GeV, $M_{\tilde{L}/\tilde{E}} = 130$ GeV $M_{\tilde{Q}/\tilde{U}/\tilde{D}_{1,2}} = 1200$ GeV, $M_{\tilde{Q}_3} = 800$ GeV, $M_{\tilde{U}_3} = 600$ GeV, $M_{\tilde{D}_3} = 1000$ GeV, $A_t = 1300$ GeV $A_\tau = A_b = 1000$ GeV, $M_2 = 230$ GeV, $m_{\tilde{g}} = 1500$ GeV, $A_\lambda = 210$ GeV, $\lambda = 0.55$, $\kappa = 0.31$, and we vary A_κ. These parameters are allowed by `HiggsBounds` everywhere apart from -145 GeV $\lesssim A_\kappa \lesssim -105$ GeV, and the Higgs signal can be interpreted as either h_1 or h_2. The left plot shows the prediction for M_{h_1} (solid curve) and M_{h_2} (dashed). The corresponding singlet components U_{13}^2 (solid) and U_{23}^2 (dashed) are shown in the middle plot. The third $\mathcal{CP}$-even Higgs is heavy and has a negligible singlet component. For $A_\kappa \lesssim -120$ GeV, h_2 is doublet-like and has a mass in the region of the observed Higgs signal (indicated by the blue band). In the MSSM, scenarios which allow the interpretation of the Higgs signal as the heavy $\mathcal{CP}$-even Higgs involve always a (relatively) light charged Higgs (see e.g. Ref. [128]). Due to changed mass relations between the Higgs bosons, it is possible in the NMSSM to have the second lightest $\mathcal{CP}$-even Higgs at 125.09 GeV together with a heavy charged Higgs. Therefore in the NMSSM the interpretation of the Higgs signal as the second lightest $\mathcal{CP}$-even Higgs is much less constrained by the LHC results from charged Higgs searches [129, 130]. The interpretation of the Higgs signal as h_2 in this model is always accompanied by a lighter state with reduced couplings to vector bosons. In this figure the charged Higgs mass is ~ 280 GeV. For $A_\kappa \gtrsim -100$ GeV, h_1 is doublet-like and has a mass in the region of the observed Higgs signal. In the "transition" region (-150 GeV $\lesssim A_\kappa \lesssim -50$ GeV) the two light $\mathcal{CP}$-even Higgs bosons are close to each other in mass and "share" the singlet component. The right plot shows the NMSSM prediction for M_W, which is approximately flat. Accordingly, the parameter regions of A_κ corresponding to two different interpretations of the Higgs signal within the NMSSM lead to very similar predictions for the W boson mass, which are in both cases compatible with the experimental result. Even a sizeable doublet–singlet mixing has only a minor effect on the M_W prediction in this case.

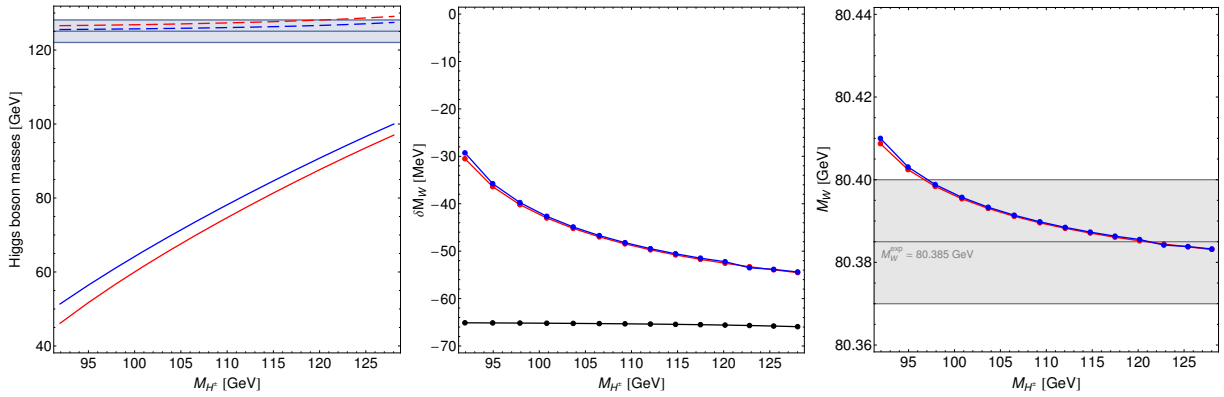

Figure 17: M_W contribution from a light charged Higgs boson. The left plot shows the prediction for the $\mathcal{CP}$-even Higgs boson masses in the NMSSM and in the MSSM as a function of the charged Higgs mass. The solid curves correspond to the mass of the lightest $\mathcal{CP}$-even Higgs in the NMSSM (blue) and the MSSM (red). The dashed curves correspond to the mass of the second lightest $\mathcal{CP}$-even Higgs in the NMSSM (blue) and the MSSM (red). The middle plot shows the shift δM_W (calculated as in Eq. (41)) induced by the Higgs and gauge boson sector in the NMSSM (blue), in the MSSM (red) and in the SM (black) with $M_{H^{\rm SM}} = M_{h_2}$. The right plot shows the W boson mass prediction in the NMSSM (blue) and the MSSM (red). The parameters used for these plots are given in the text.

We have demonstrated so far that, taking Higgs search constraints and the information on the discovered Higgs signal into account,[21] the genuine NMSSM effects from the extended Higgs sector are quite small, and the Higgs sector contributions that we analysed so far were dominated by SM-type contributions. This is true in the absence of a light charged Higgs boson, as we will discuss now. Light charged Higgs bosons (together with a light $\mathcal{CP}$-even Higgs with small but non-zero couplings to vector bosons) can lead to sizeable (non SM-like) Higgs contributions to M_W. This effect can also be observed in the MSSM. Although it is not a genuine NMSSM effect, we want to demonstrate the impact of such a contribution here. For Fig. 17 we choose the following parameters $m_t = 173.34$ GeV, $\tan\beta = 9.25$, $\mu = 200$ GeV, $M_{\tilde{L}/\tilde{E}} = 300$ GeV $M_{\tilde{Q}/\tilde{U}/\tilde{D}_{1,2}} = 1500$ GeV, $M_{\tilde{Q}_3} = M_{\tilde{U}_3} = M_{\tilde{D}_3} = 1100$ GeV, $A_t = -2300$ GeV $A_\tau = A_b = -1500$ GeV, $M_2 = 500$ GeV, $m_{\tilde{g}} = 1500$ GeV, $\lambda = 0.2$, $\kappa = 0.6$, $A_\kappa = -1370$ GeV, and we vary $\hat{m}_A$. The left plot in Fig. 17 shows the predictions for the masses of the lightest two $\mathcal{CP}$-even Higgs bosons in the NMSSM (blue) and in the MSSM (red) as a function of the charged Higgs mass. In both models the second lightest Higgs falls in the mass range 125.09 ± 3.04 GeV for the chosen parameters. This scenario is essentially excluded by the latest charged Higgs searches [129,130]. Nevertheless, we include these plots to illustrate the possible size of the contributions from a light charged Higgs.

The middle plot shows the shift δM_W calculated as in Eq. (41) with x=gauge-boson/Higgs in the NMSSM (blue) and in the MSSM (red) while the right plot shows the full M_W prediction in the NMSSM (blue) and in the MSSM (red). As one can see the MSSM and NMSSM contributions to M_W are very similar. Since the masses of charginos, neutralinos and sfermions stay constant when varying $\hat{m}_A$ (or $M_{H^\pm}$), the change in M_W with $M_{H^\pm}$ stems purely from the Higgs sector. The Higgs sector contribution to M_W comes dominantly from the light charged Higgs, while the lightest $\mathcal{CP}$-even Higgs

[21] Neglecting those experimental bounds one could have very light $\mathcal{CP}$-Higgs bosons with only a small singlet component, which would give large contributions to M_W. However this possibility will not be discussed here.

gives only a rather small contribution to M_W due to its reduced vector boson couplings. In the middle plot the SM result for δM_W with $M_{H^{\rm SM}} = M_{h_2}$ is shown in black. A significant difference between the SM Higgs contribution and the MSSM/NMSSM Higgs contributions can be observed. As one can see in the right plot, the displayed variation with the charged Higgs boson mass corresponds to about a 1σ shift in M_W.

4.4.4 Neutralino sector contributions

We start the discussion of the contributions from the NMSSM neutralino sector, which differs from the respective MSSM sector, with Fig. 18. We choose the parameters $m_t = 173.34$ GeV, $\tan\beta = 3$, $\mu = 200$ GeV, $M_{\tilde{L}/\tilde{E}} = 1000$ GeV, $M_{\tilde{Q}/\tilde{U}/\tilde{D}_{1,2}} = 1500$ GeV, $M_{\tilde{Q}_3} = M_{\tilde{U}_3} = 650$ GeV, $M_{\tilde{D}_3} = 1000$ GeV, $A_t = A_\tau = A_b = 1000$ GeV, $m_{\tilde{g}} = 1500$ GeV, $A_\lambda = 580$ GeV, $\lambda = 0.64$, $\kappa = 0.25$, $A_\kappa = -10$ GeV, and we vary M_2. In the upper left plot, the blue curve shows the $M_W^{\rm NMSSM}$ prediction and the red curve the $M_W^{\rm MSSM}$ prediction. The difference between the NMSSM prediction and the MSSM prediction is small for $M_2 \lesssim 200$ GeV and increases for larger M_2 values. The origin of this difference is investigated in the other three plots of Fig. 18. As before our procedure to identify an MSSM point which can be compared to the NMSSM point implies different predictions for the lightest $\mathcal{CP}$-even Higgs mass. Here we subtract again the difference in the SM contributions, arising from the different Higgs mass predictions. The additional blue dashed curve (with open dots) in the upper right plot of Fig. 18 corresponds to $M_W^{\rm NMSSM,\,sub} = M_W^{\rm NMSSM} - M_W^{\rm SM}(M_{h_1}) + M_W^{\rm SM}(M_h)$. For large M_2 the difference between the NMSSM and the MSSM prediction for M_W can be fully explained by the difference in the (SM-type) Higgs mass contributions, which arise from inserting different predictions for M_{h_1} and M_h. However after subtracting the difference from the Higgs mass contributions we observe a sizeable difference between $M_W^{\rm NMSSM,\,sub}$ and $M_W^{\rm MSSM}$ for small M_2. This difference stems from different sizes of the chargino/neutralino sector contributions between the two SUSY models, which tend to compensate the difference between $M_W^{\rm NMSSM}$ and $M_W^{\rm MSSM}$ arising from the Higgs sector. This can be seen in the lower left plot, where we display the shift δM_W (calculated as in Eq. (41)) induced by the chargino/neutralino contributions in the MSSM (red) and in the NMSSM (blue). At $M_2 = 160$ GeV the chargino mass is 108 GeV and thus just above the LEP limit. The δM_W contribution from the chargino/neutralino sector in the MSSM reaches 8.5 MeV in this case.[22] In the NMSSM the maximal δM_W contribution from the chargino/neutralino sector is 16.5 MeV — significantly larger than in the MSSM. Both in the MSSM and the NMSSM, the chargino/neutralino contributions decrease when increasing M_2 and therewith the chargino and neutralino masses, showing the expected behaviour when decoupling the gaugino sector. The largest difference between the NMSSM and the MSSM chargino/neutralino contributions is ~ 8 MeV (at $M_2 = 160$ GeV). The difference arises from the neutralino sector, since the chargino sector is unchanged in the NMSSM with respect to the MSSM. We will discuss in more detail below why the contributions from the neutralino sector are larger in the NMSSM than in the MSSM. The lower right plot of Fig. 18 is similar to the upper right plot, but it contains a fourth curve (blue dotted with open diamonds) which was obtained by subtracting the different chargino/neutralino contributions, thus it corresponds to $M_W^{\rm NMSSM,sub} - \delta M_W^{\rm NMSSM} + \delta M_W^{\rm MSSM}$. This curve lies very close to the MSSM prediction. We have therefore identified the contributions causing the difference between the $M_W^{\rm NMSSM}$ and the $M_W^{\rm MSSM}$ predictions.

We continue with the discussion of the neutralino contributions to M_W in the NMSSM in Fig. 19.

[22] This is not the maximal effect possible for the chargino/neutralino contributions in the MSSM. The chargino/neutralino contributions depend on the slepton masses (see diagrams in Figs. 5-7). For lighter slepton masses the chargino/neutralino contributions in the MSSM can reach up to 20 MeV, as analysed in Ref. [61].

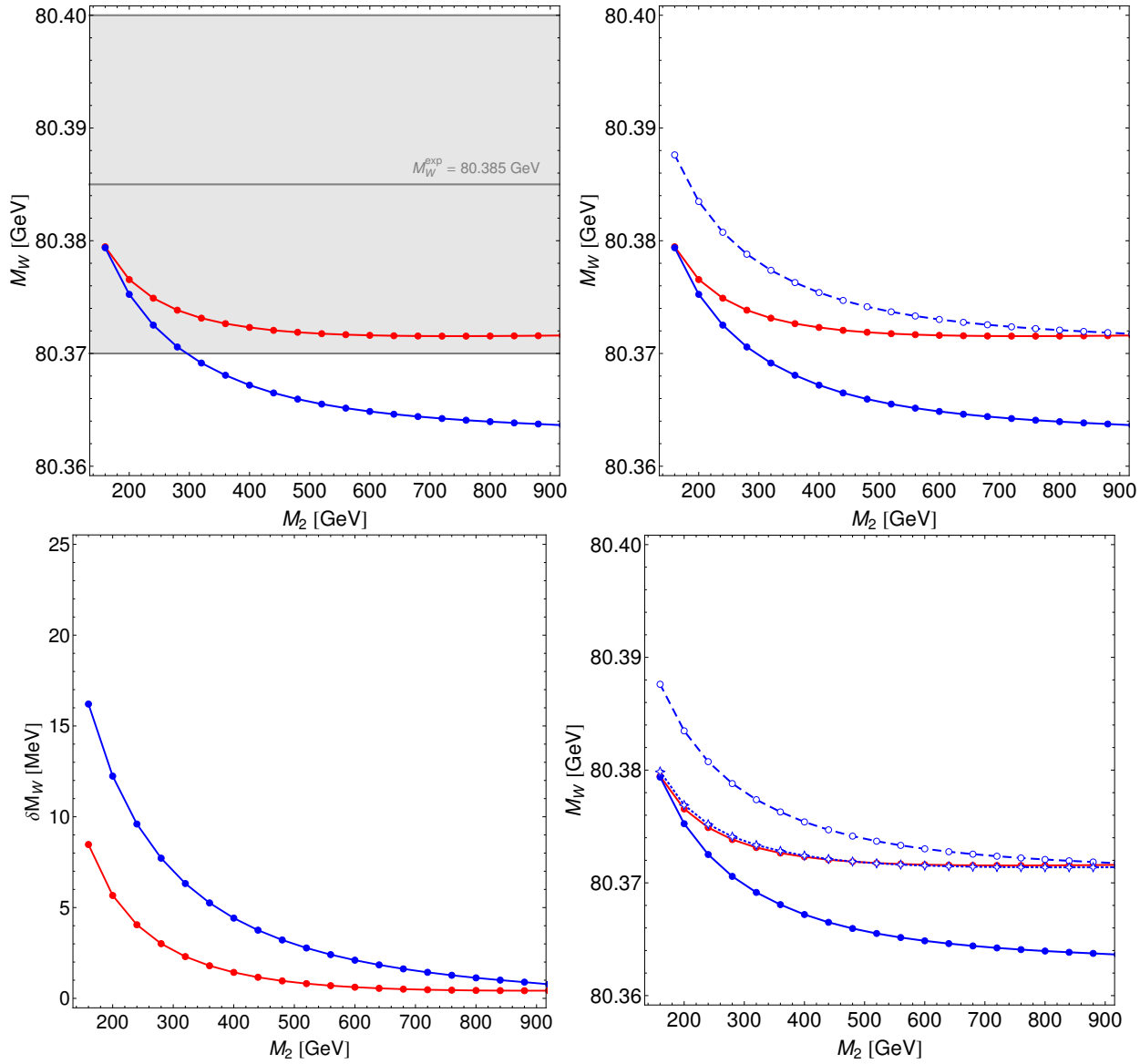

Figure 18: The upper left plot shows the $M_W^{\rm NMSSM}$ prediction (blue) and the $M_W^{\rm MSSM}$ prediction (red) as a function of M_2. The experimental M_W measurement is indicated as a grey band. The upper right plot shows additionally a dashed blue curve (open dots) corresponding to $M_W^{\rm NMSSM,\,sub} = M_W^{\rm NMSSM} - M_W^{\rm SM}(M_{h_1}) + M_W^{\rm SM}(M_h)$. The lower left plot shows the shift in the W boson mass δM_W (calculated as in Eq. (41) with x=chargino/neutralino) in the MSSM (red) and in the NMSSM (blue). The lower right plot is similar to the upper right plot but it additionally contains the dotted blue curve (open diamonds) which corresponds to $M_W^{\rm NMSSM,\,sub} - \delta M_W^{\rm NMSSM} + \delta M_W^{\rm MSSM}$ where δM_W is the shift in M_W induced by the chargino/neutralino contributions. The NMSSM parameter points are allowed by `HiggsBounds`, and M_{h_1} falls in the range 125.09 ± 3.04 GeV for $M_2 \lesssim 725$ GeV. The parameters used for these plots are given in the text.

The chosen parameters are $m_t = 173.34$ GeV, $\tan\beta = 5.5$, $\mu = 200$ GeV, $M_{\tilde{L}/\tilde{E}} = 245$ GeV,

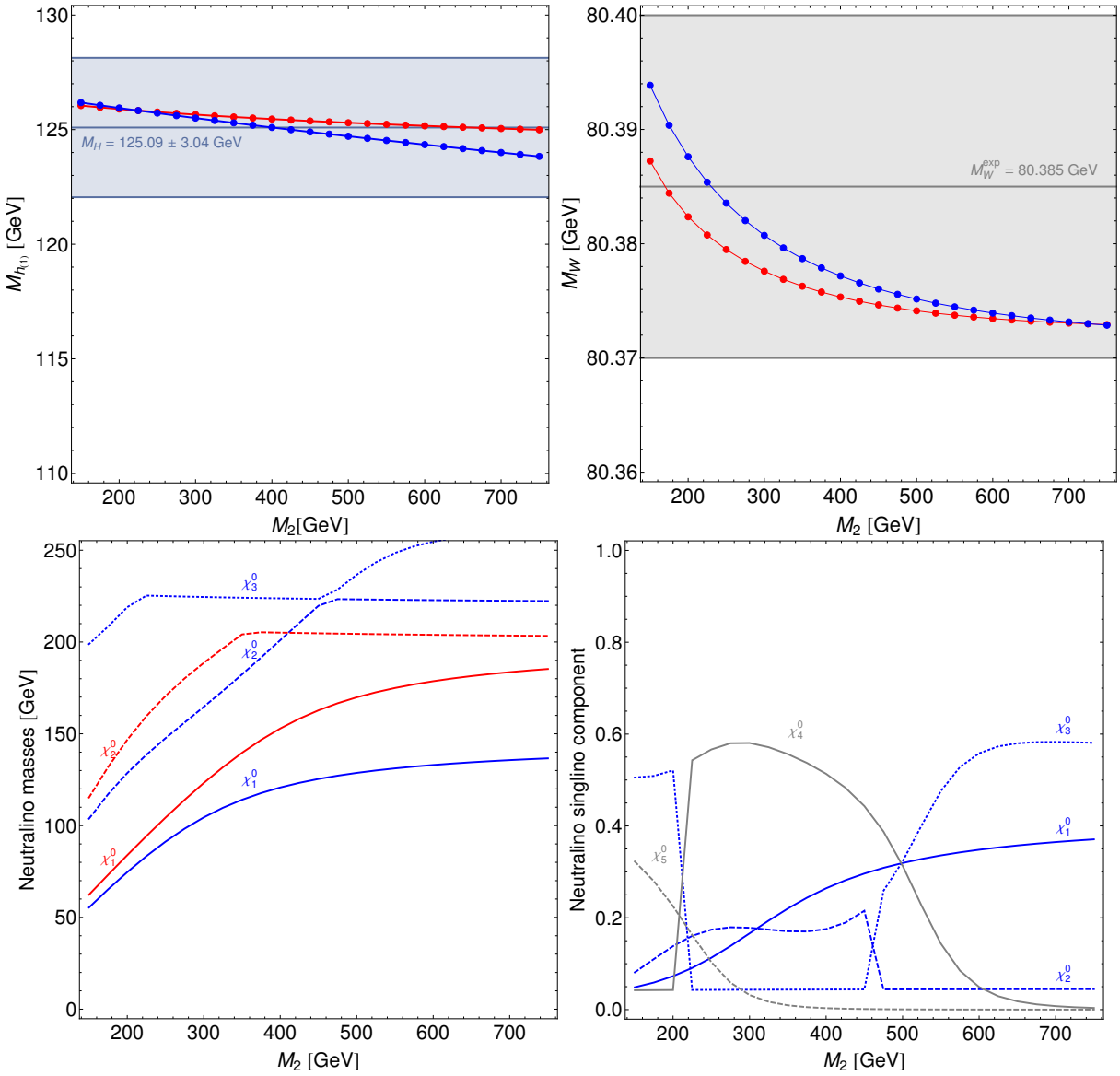

Figure 19: The upper left plot shows the masses of the lightest $\mathcal{CP}$-even Higgs boson in the NMSSM (blue) and the MSSM (red) as a function of M_2. The upper right plot shows the prediction for $M_W^{\rm NMSSM}$ (blue) and for $M_W^{\rm MSSM}$ (red). The lightest three neutralino masses and the neutralino singlet components are displayed in the lower row. The parameters (given in the text) are chosen such that the Higgs sectors of the MSSM and the NMSSM are very similar to each other. The parameter region in both models is allowed by `HiggsBounds` and predicts the lightest $\mathcal{CP}$-even Higgs (which is SM-like) close to 125.09 GeV.

$M_{\tilde{Q}/\tilde{U}/\tilde{D}_{1,2}} = 1500$ GeV, $M_{\tilde{Q}_3} = M_{\tilde{U}_3} = M_{\tilde{D}_3} = 1000$ GeV, $A_t = A_\tau = A_b \simeq 1964$ GeV, $m_{\tilde{g}} = 1500$ GeV, $\hat{m}_A = 1200$ GeV, $\lambda = 0.62$, $\kappa = 0.3$, $A_\kappa = -10$ GeV, and M_2 is varied. All parameter points are `HiggsBounds` allowed. Again we get the MSSM prediction by setting the `FeynHiggs` $M_{H^\pm}$ input to the value of the charged Higgs mass calculated by `NMSSMTools`. For this set of parameters

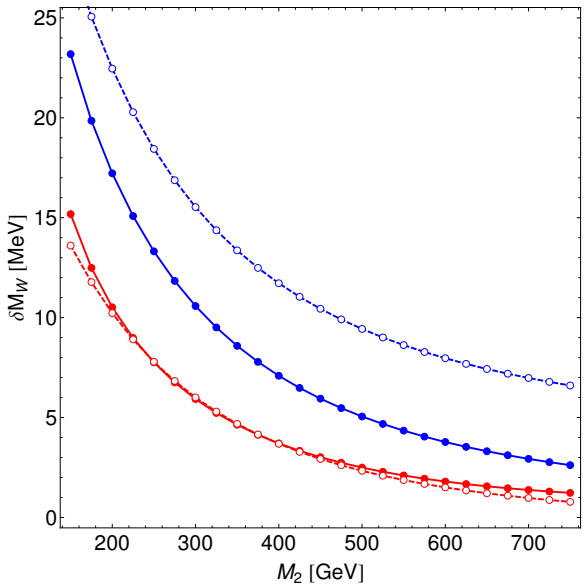

Figure 20: The shifts δM_W in the NMSSM (blue) and in the MSSM (red), calculated taking the full chargino/neutralino contribution to Δr into account (solid) and using only the $\Delta\rho$ approximation (dashed). The parameters are chosen as in Fig. 19.

this procedure leads to a scenario where the MSSM and the NMSSM Higgs boson sectors are very similar to each other. Both models predict the lightest $\mathcal{CP}$-even Higgs close to the experimental value 125.09 GeV, as one can see in the upper left plot of Fig. 19 showing the masses of the two states M_h (MSSM, red) and M_{h_1} (NMSSM, blue). The difference between M_h and M_{h_1} is $\lesssim 1$ GeV, resulting in a small ($\mathcal{O}(1$ MeV)) difference in M_W from the Higgs sector contributions. The upper right plot of Fig. 19 displays the W boson mass prediction in the NMSSM (blue) and in the MSSM (red). The difference between these two predictions is largest (7 MeV) for $M_2 = 150$ GeV and (almost) vanishes for large M_2. Since differences in the Higgs sector contributions are quite small, the difference between $M_W^{\rm NMSSM}$ and $M_W^{\rm MSSM}$ arises predominately from the differences in the neutralino sector. We note that in this scenario both M_{h_1} and M_W lie within the preferred regions indicated by the blue and grey bands for the whole parameter range displayed in the figure.

In order to investigate the reasons for the different predictions for the chargino/neutralino contributions we plot the masses of the three lightest neutralino states in the NMSSM (blue) and the MSSM (red) in the lower left plot. The other MSSM/NMSSM neutralinos are heavier than 250 GeV and hardly affect the M_W prediction. We set here the (unphysical) soft masses M_1 and M_2 equal in the MSSM and the NMSSM and identify the MSSM μ parameter with the effective μ of the NMSSM. The resulting predictions for the masses of $\tilde{\chi}_1^0$ and $\tilde{\chi}_2^0$ are a few GeV lower in the NMSSM than in the MSSM. The singlino components of the NMSSM neutralinos, $|N_{i5}|^2$, where N was defined in Eq. (15), are shown in the lower right plot, and we can observe a strong mixing between the five states. The singlino components of $\tilde{\chi}_1^0$ and $\tilde{\chi}_2^0$ are below 10% for $M_2 = 150$ GeV and increase up to 40%(20%) for $\tilde{\chi}_1^0(\tilde{\chi}_2^0)$ for higher M_2 values. The lighter neutralino states (with relatively small singlino component) lead to larger contributions from the neutralino sector to M_W in the NMSSM compared to the MSSM.

In the next step we analyse how well the full Δr contribution of the chargino/neutralino sector can be approximated by taking into account only the leading term $-c_W^2/s_W^2\,\Delta\rho$ (defined in Eq. (26)). The

$\Delta\rho$ term contains only the W and Z boson self-energies at zero momentum transfer, thus this approximation neglects in particular the contributions from box, vertex and fermion self-energy diagrams containing charginos and neutralinos. The $\Delta\rho$ term corresponds to the T parameter of the S, T, U parameters [131, 132], often used to parametrize new physics contribution to electroweak precision observables. For the plot in Fig. 20 we use the same parameters as in Fig. 19. Again the blue(red) solid curve shows the δM_W shift as a function of M_2, calculated as in Eq. (41) with x=chargino/neutralino in the NMSSM(MSSM) (the two solid curves are identical to the ones in the upper right plot of Fig. 19). The two dashed curves show the M_W contributions in the NMSSM (blue) and in the MSSM (red) obtained when the full $\Delta r^{\text{chargino/neutralino}(\alpha)}$ is approximated by the chargino and neutralino contributions to the $\Delta\rho$ parameter:

$$\delta M_W = -\frac{M_W^{\text{ref}}}{2} \frac{s_W^2}{c_W^2 - s_W^2} \left(-\frac{c_W^2}{s_W^2}\right) \Delta\rho^{\text{chargino/neutralino}}. \tag{42}$$

In the MSSM the $\Delta\rho$ term containing charginos and neutralinos provides a very good approximation of the full Δr term in the intermediate range 200 GeV $\lesssim M_2 \lesssim$ 500 GeV. In the range of small and large M_2 values, $\Delta\rho$ slightly underestimates the full Δr contribution, the difference here is ~ 1.5 MeV for $M_2 = 150$ GeV and ~ 0.5 MeV for $M_2 = 750$ GeV. In the NMSSM the $\Delta\rho$ term gives a δM_W contribution which is larger ($\gtrsim 4$ MeV) than the full Δr result for the full M_2 range plotted here. It should be noted that the chargino/neutralino sector does not completely decouple for large M_2 in this case, which is a consequence of the presence of a light Higgsino, $\mu = 200$ GeV. For $M_2 = 750$ GeV the lightest neutralino has a mass of $M_2 = 140$ GeV, with a singlino component of $\sim 40\%$ and a Higgsino component of $\sim 60\%$. In this scenario the singlino-higgsino mixing leads to a positive contribution to $\Delta\rho$, but to a negative contribution to the Δr terms beyond $\Delta\rho$ (we checked that the contribution from the box diagrams is negligible for large M_2 values). We also checked that going to large μ values, the chargino/neutralino sector decouples and all terms vanish. In this scenario the two effects largely cancel each other and for large M_2 one finds a small positive value for the full Δr result. This however depends on the chosen parameters and the admixture of the light neutralino, e.g. in the scenario discussed in Fig. 15 the negative contributions exceed the positive ones so that the full Δr result is negative for large M_2. Thus, we have shown that the $\Delta\rho$ approximation for the chargino and neutralino contributions works quite well in the MSSM, whereas sizeable corrections to M_W beyond the $\Delta\rho$ approximation can occur in the NMSSM.

As a final step we want to discuss the dependence of the M_W prediction in the NMSSM on the μ parameter, which enters both in the sfermion and in the chargino/neutralino sectors. The left plot of Fig. 21 shows the W boson mass prediction in the NMSSM as a function of μ, with the parameters chosen as $m_t = 173.34$ GeV, $\tan\beta = 20$, $M_{\tilde{L}/\tilde{E}} = 250$ GeV, $M_{\tilde{Q}/\tilde{U}/\tilde{D}_{1,2}} = 1500$ GeV, $M_{\tilde{Q}_3} = 500$ GeV $M_{\tilde{U}_3} = 1500$ GeV, $M_{\tilde{D}_3} = 300$ GeV, $A_\tau = 0$ GeV, $A_t = A_b = -2185$ GeV, $M_2 = 150$ GeV, $m_{\tilde{g}} = 1500$ GeV, $\hat{m}_A = 1500$ GeV, $\lambda = 0.2$, $\kappa = 0.6$, $A_\kappa = -1370$ GeV. The parameter points are `HiggsBounds` allowed, and h_1 falls in the mass range 125.09 ± 3.04 GeV. When increasing μ, the M_W^{NMSSM} prediction decreases first, reaches its minimum for $\mu \sim 1100$ GeV and then rapidly increases. This behaviour can be explained by looking at the contributions to M_W from the chargino/neutralino sector (here we take again the full Δr contributions into account) and from the stop/sbottom sector. The shift δM_W arising from charginos and neutralinos is shown in the middle plot of Fig. 21. The chargino/neutralino contribution is largest for small μ and decreases with increasing μ. Going to larger μ the masses of the (higgsino-like) chargino and neutralino states increase and the M_W contribution decreases. The shift δM_W arising from the stop/sbottom sector is shown in the right plot of Fig. 21. The contributions from the stop/sbottom sector (dominated by the $\Delta\rho$ contri-

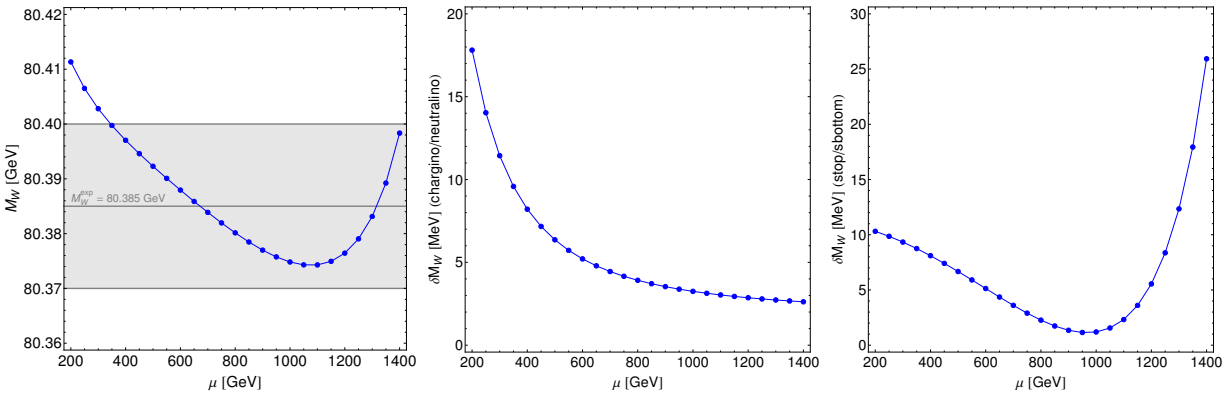

Figure 21: Dependence of the W boson mass prediction in the NMSSM on the μ parameter. The left plot shows the $M_W^{\rm NMSSM}$ prediction, the middle one the δM_W contribution from the chargino/neutralino sector and the right one shows the δM_W contribution from the stop/sbottom sector. The parameters are given in the text.

butions) get smaller when μ is increased up to $\mu \sim 1000$ GeV and then start to rise if μ is increased further. Increasing μ, the splitting between the two sbottoms gets larger (while the stop masses stay nearly constant), which implies also an increase of the splitting between stops and sbottoms. The counteracting terms in $\Delta\rho$ (see the discussion in Sect. 4.4.1) lead to the observed behaviour.

5 Conclusions

We have presented the currently most accurate prediction for the W boson mass in the NMSSM, in terms of the Z boson mass, the fine-structure constant, the Fermi constant, and model-parameters entering via higher-order contributions. This result includes the full one-loop determination and all available higher-order corrections of SM and SUSY type. These improved predictions have been compared to the state–of–the–art predictions in the SM and the MSSM within a coherent framework, and we have presented numerical results illustrating the similarities and the main differences between the predictions of these models.

Within the SM, interpreting the signal discovered at the LHC as the SM Higgs boson with $M_{H^{\rm SM}} = 125.09$ GeV, there is no unknown parameter in the M_W prediction anymore. We have updated the SM prediction for M_W making use of the most up to date higher-order contributions. For $M_{H^{\rm SM}} = 125.09$ GeV this yields $M_W^{\rm SM} = 80.358$ GeV (with a theory uncertainty from unknown higher-order corrections of about 4 MeV). The comparison with the current experimental value of $M_W^{\rm exp} = 80.385 \pm 0.015$ GeV shows the well-known feature that the SM prediction lies somewhat below the value that is preferred by the measurements from LEP and the Tevatron (at the level of about $1.8\,\sigma$). The loop contributions from supersymmetric particles in general give rise to an upward shift in the prediction for M_W as compared to the SM case, which tend to bring the prediction into better agreement with the experimental result.

For the calculation of the M_W prediction, we made use of the highly automated programs `FeynArts` and `FormCalc`. Our evaluation is based on a framework which was developed in Ref. [6], consisting in particular of a NMSSM model file for the program `FeynArts` and a `Fortran` driver for the evaluation of the masses, mixing angles, etc. needed for the numerical evaluation. The code `NMSSMTools` is used

for the evaluation of the loop-corrected Higgs boson masses. The implementation of another result for the NMSSM Higgs masses, obtained in Ref. [117], is in progress.

Our improved prediction for the W boson mass in the NMSSM consists of the full one-loop result, all available higher-order corrections of SM-type, stop-loop and sbottom-loop contributions with gluon and gluino exchange of $\mathcal{O}(\alpha\alpha_s)$, relevant reducible higher-order contributions, as well as an approximate treatment of the MSSM-type Yukawa-enhanced electroweak two-loop corrections of $\mathcal{O}(\alpha_t^2)$, $\mathcal{O}(\alpha_t\alpha_b)$, $\mathcal{O}(\alpha_b^2)$. Analytic expressions for all those contributions are implemented, except for the electroweak two-loop contributions of SM-type, for which we make use of the fit formula given in Ref. [59]. The latter allows us to properly evaluate $\Delta r^{\rm SM}$ at an NMSSM value for the W boson mass.

We presented a detailed investigation of the prediction for $M_W^{\rm NMSSM}$, focussing on the parameter regions which are allowed by Higgs searches (tested by `HiggsBounds`), SUSY searches and further theoretical constraints. As a first step we analysed the size of the contributions from stops/sbottoms. Since the sfermion sector is unchanged in the NMSSM with respect to the MSSM, we have done this study in the MSSM limit, yielding an important check of our NMSSM implementation. We have investigated the size of the SUSY two-loop corrections to M_W and found that the $\mathcal{O}(\alpha\alpha_s)$ corrections beyond the pure gluon exchange contributions, which were incorporated in the previous result of Ref. [78], can give sizeable contributions. On the other hand, the effect of the Yukawa-enhanced electroweak two-loop corrections of $\mathcal{O}(\alpha_t^2)$, $\mathcal{O}(\alpha_t\alpha_b)$, $\mathcal{O}(\alpha_b^2)$ stays numerically relatively small in the allowed parameter region.

Concerning the investigation of genuine NMSSM effects, we started our discussion with the Higgs sector contributions to M_W. The tree-level prediction for the lightest $\mathcal{CP}$-even Higgs mass is modified by an additional term in the NMSSM as compared to the MSSM, which (for small $\tan\beta$) leads to an upward shift of the tree-level Higgs mass. Therefore, in that region, the radiative corrections needed to push the Higgs mass to about 125 GeV can be smaller than in the MSSM, which implies that lighter stop masses and a smaller stop mixing are possible. We investigated a scenario where this additional tree-level term gives rise to a higher M_{h_1} prediction than in the MSSM limit. The impact on the M_W prediction is a downward shift (of ~ 25 MeV in the considered example) as compared to the corresponding prediction in the MSSM. In the prediction for M_W this contribution from the Higgs sector enters together with other SUSY loop contribution to Δr yielding an upward shift in M_W compared to the SM. The overall effect is such that also in a scenario of this kind a very good agreement between the theoretical prediction and the experimental result can be reached. We have furthermore investigated the effect of doublet–singlet mixing. While a sizeable doublet–singlet mixing can occur in the region where the two NMSSM Higgs states h_1 and h_2 are close to each other in mass, we find that it has only a minor effect on the M_W prediction.

In the NMSSM the Higgs signal seen at the LHC can be interpreted both as the lightest and the second-lightest $\mathcal{CP}$-even Higgs boson of the spectrum. Both interpretations give predictions for the W boson mass in good agreement with the M_W measurement. In the NMSSM the interpretation of the LHC signal as the second-lightest $\mathcal{CP}$-even Higgs h_2 is possible together with a relatively heavy charged Higgs. This is different from the situation in the MSSM, where all Higgs states have to be light in this case, so that such a scenario can be probed by searches for charged Higgs bosons in top-quark decays. As a consequence, the interpretation of the observed Higgs signal as the second-lightest $\mathcal{CP}$-even Higgs boson is much less constrained in the NMSSM compared to the MSSM.

For completeness, we have nevertheless briefly investigated also the case of a light charged Higgs boson. We have found that a light charged Higgs boson (together with a light $\mathcal{CP}$-even Higgs with reduced but non-zero couplings to gauge bosons) can in principle give very significant contributions to M_W (as in the MSSM). In that case large deviations from the SM Higgs sector contributions occur,

but as discussed above scenarios of this kind are severely constrained by limits from charged Higgs searches at the LHC. Generally we find that taking all available constrains on the Higgs sector into account, the specific NMSSM effects of the Higgs sector to M_W are relatively small.

On the other hand, the extended neutralino sector of the NMSSM can lead to a sizeable difference between the W boson mass predictions in the NMSSM and the MSSM. The chargino/neutralino contributions to M_W can be larger in the NMSSM compared to the MSSM, where in the scenario which we studied the difference reaches ~ 8 MeV. Assuming the same values for the soft mass parameters in the MSSM and the NMSSM and choosing $\mu = \mu_{\text{eff}}$, the mixing with the singlino leads to shifts in the neutralino masses as compared to the MSSM case. In the considered scenarios the lightest NMSSM states turned out to be lighter than the corresponding MSSM states. They also have a relatively small singlino component, which causes the resulting contributions to the prediction for M_W to be larger than in the MSSM. While light wino/bino states typically give positive contributions, light higgsinos can give contributions entering with both signs.

As a final step of our analysis, we compared the M_W prediction calculated with the full Δr to the one where the full result is approximated by the contribution to $\Delta\rho$. We found that the difference between the full result and the $\Delta\rho$ approximation can be sizeable in the NMSSM, where the approximation can lead both to an over- or an underestimate of the full result. Light neutralinos with a significant higgsino–singlino mixing tend to give a positive contribution to $\Delta\rho$, but a negative contribution to the Δr terms beyond $\Delta\rho$. It therefore depends on the exact patterns of the admixture with the singlino whether the neutralino sector of the NMSSM leads to an upward or downward shift in the prediction for M_W in comparison with the MSSM.

We have demonstrated that the prediction for the W boson mass arising from the relation with the Z boson mass, the Fermi constant and the fine structure constant in comparison with high-precision measurements of those quantities provides a high sensitivity for discriminating between the SM and possible extensions of it. With further improvements of the experimental accuracy of M_W, possible improvements in the determination of m_t and further information on possible mass spectra of supersymmetric particles – either via improved limits or the discovery of new states – the impact of this important tool can be expected to be even more pronounced in the future.

Acknowledgements

We are grateful to Florian Domingo for helpful discussions and for providing numerical values to cross-check our results. We also thank Ayres Freitas, Thomas Hahn, Sven Heinemeyer, Wolfgang Hollik and Pietro Slavich for helpful discussions. This work has been supported by the Collaborative Research Center SFB676 of the DFG, "Particles, Strings and the early Universe". O.S. is supported by the Swedish Research Council (VR) through the Oskar Klein Centre. This work is part of the D-ITP consortium, a program of the Netherlands Organization for Scientific Research (NWO) that is funded by the Dutch Ministry of Education, Culture and Science (OCW). This research was supported in part by the European Commission through the "HiggsTools" Initial Training Network PITN-GA-2012-316704.

References

[1] **ATLAS** Collaboration, G. Aad et al., *Observation of a new particle in the search for the Standard Model Higgs boson with the ATLAS detector at the LHC*, *Phys.Lett.* **B716** (2012) 1–29, [arXiv:1207.7214].

[2] **CMS** Collaboration, S. Chatrchyan et al., *Observation of a new boson at a mass of 125 GeV with the CMS experiment at the LHC*, *Phys.Lett.* **B716** (2012) 30–61, [arXiv:1207.7235].

[3] J. E. Kim and H. P. Nilles, *The mu Problem and the Strong CP Problem*, *Phys.Lett.* **B138** (1984) 150.

[4] U. Ellwanger, C. Hugonie, and A. M. Teixeira, *The Next-to-Minimal Supersymmetric Standard Model*, *Phys.Rept.* **496** (2010) 1–77, [arXiv:0910.1785].

[5] U. Ellwanger, *Enhanced di-photon Higgs signal in the Next-to-Minimal Supersymmetric Standard Model*, *Phys.Lett.* **B698** (2011) 293–296, [arXiv:1012.1201].

[6] R. Benbrik, M. Gomez Bock, S. Heinemeyer, O. Stål, G. Weiglein, and L. Zeune, *Confronting the MSSM and the NMSSM with the Discovery of a Signal in the two Photon Channel at the LHC*, *Eur.Phys.J.* **C72** (2012) 2171, [arXiv:1207.1096].

[7] S. King, M. Mühlleitner, R. Nevzorov, and K. Walz, *Natural NMSSM Higgs Bosons*, *Nucl.Phys.* **B870** (2013) 323–352, [arXiv:1211.5074].

[8] K. Choi, S. H. Im, K. S. Jeong, and M. Yamaguchi, *Higgs mixing and diphoton rate enhancement in NMSSM models*, *JHEP* **1302** (2013) 090, [arXiv:1211.0875].

[9] T. Schörner-Sadenius, *The Large Hadron Collider: Harvest of Run 1*. Springer International Publishing, 2015.

[10] **ATLAS** Collaboration. See: https://twiki.cern.ch/twiki/bin/view/AtlasPublic/SupersymmetryPublicResults.

[11] **CMS** Collaboration. See: https://twiki.cern.ch/twiki/bin/view/CMSPublic/PhysicsResultsSUS.

[12] **CDF** Collaboration, F. Abe et al., *Observation of top quark production in $\bar{p}p$ collisions*, *Phys.Rev.Lett.* **74** (1995) 2626–2631, [hep-ex/9503002].

[13] **DØ** Collaboration, S. Abachi et al., *Observation of the top quark*, *Phys.Rev.Lett.* **74** (1995) 2632–2637, [hep-ex/9503003].

[14] **CDF** Collaboration, T. Aaltonen et al., *Precise measurement of the W-boson mass with the CDF II detector*, *Phys.Rev.Lett.* **108** (2012) 151803, [arXiv:1203.0275].

[15] **D0** Collaboration, V. M. Abazov et al., *Measurement of the W Boson Mass with the D0 Detector*, *Phys.Rev.Lett.* **108** (2012) 151804, [arXiv:1203.0293].

[16] **Tevatron Electroweak Working Group**, *2012 Update of the Combination of CDF and DØ Results for the Mass of the W Boson*, arXiv:1204.0042.

[17] **ALEPH, DELPHI, L3, OPAL, SLD, LEP Electroweak Working Group, SLD Electroweak Group, SLD Heavy Flavour Group**, S. Schael, et al., *Precision electroweak measurements on the Z resonance*, *Phys.Rept.* **427** (2006) 257–454, [hep-ex/0509008].
See: http://lepewwg.web.cern.ch/LEPEWWG/.

[18] S. Heinemeyer, S. Kraml, W. Porod, and G. Weiglein, *Physics impact of a precise determination of the top quark mass at an e^+e^- linear collider*, *JHEP* **0309** (2003) 075, [hep-ph/0306181].

[19] **Tevatron Electroweak Working Group, CDF, DØ**, *Combination of CDF and DØ results on the mass of the top quark using up to 5.8 fb-1 of data*, arXiv:1107.5255.

[20] **ATLAS, CMS** Collaborations. ATLAS-CONF-2013-102, CMS PAS TOP-13-005.

[21] **ATLAS** Collaboration. ATLAS-CONF-2013-046.

[22] **ATLAS** Collaboration. ATLAS-CONF-2013-077.

[23] **ATLAS** Collaboration, G. Aad et al., *Measurement of the top quark mass in the $t\bar{t} \to$ lepton + jets and $t\bar{t} \to$ dilepton channels using $\sqrt{s} = 7$ TeV ATLAS data*, arXiv:1503.05427.

[24] **CMS** Collaboration, S. Chatrchyan et al., *Measurement of the top-quark mass in $t\bar{t}$ events with lepton+jets final states in pp collisions at $\sqrt{s} = 7$ TeV*, *JHEP* **1212** (2012) 105, [arXiv:1209.2319].

[25] **CMS** Collaboration, S. Chatrchyan et al., *Measurement of the top-quark mass in $t\bar{t}$ events with dilepton final states in pp collisions at $\sqrt{s} = 7$ TeV*, *Eur.Phys.J.* **C72** (2012) 2202, [arXiv:1209.2393].

[26] **CMS** Collaboration, S. Chatrchyan et al., *Measurement of the top-quark mass in all-jets $t\bar{t}$ events in pp collisions at $\sqrt{s}$=7 TeV*, *Eur.Phys.J.* **C74** (2014), no. 4 2758, [arXiv:1307.4617].

[27] **ATLAS, CDF, CMS, DØ** Collaborations, *First combination of Tevatron and LHC measurements of the top-quark mass*, arXiv:1403.4427.

[28] P. Z. Skands and D. Wicke, *Non-perturbative QCD effects and the top mass at the Tevatron*, *Eur.Phys.J.* **C52** (2007) 133–140, [hep-ph/0703081].

[29] A. H. Hoang and I. W. Stewart, *Top Mass Measurements from Jets and the Tevatron Top-Quark Mass*, *Nucl.Phys.Proc.Suppl.* **185** (2008) 220–226, [arXiv:0808.0222].

[30] A. H. Hoang, *The Top Mass: Interpretation and Theoretical Uncertainties*, arXiv:1412.3649.

[31] G. Moortgat-Pick, H. Baer, M. Battaglia, G. Belanger, K. Fujii, et al., *Physics at the e^+e^- Linear Collider*, arXiv:1504.01726.

[32] M. Baak, A. Blondel, A. Bodek, R. Caputo, T. Corbett, et al., *Study of Electroweak Interactions at the Energy Frontier*, arXiv:1310.6708.

[33] A. Sirlin, *Radiative Corrections in the $SU(2)_L \times U(1)$ Theory: A Simple Renormalization Framework*, *Phys.Rev.* **D22** (1980) 971–981.

[34] W. Marciano and A. Sirlin, *Radiative Corrections to Neutrino Induced Neutral Current Phenomena in the $SU(2)_L \times U(1)$ Theory*, *Phys.Rev.* **D22** (1980) 2695.

[35] A. Djouadi and C. Verzegnassi, *Virtual Very Heavy Top Effects in LEP / SLC Precision Measurements*, *Phys. Lett.* **B195** (1987) 265.

[36] A. Djouadi, *$\mathcal{O}(\alpha\alpha_s)$ Vacuum Polarization Functions of the Standard Model Gauge Bosons*, *Nuovo Cim.* **A100** (1988) 357.

[37] B. Kniehl, *Two Loop Corrections to the Vacuum Polarizations in Perturbative QCD*, *Nucl. Phys.* **B347** (1990) 86.

[38] F. Halzen and B. Kniehl, *Δr beyond one loop*, *Nucl. Phys.* **B353** (1991) 567.

[39] B. Kniehl and A. Sirlin, *Dispersion relations for vacuum polarization functions in electroweak physics*, *Nucl. Phys.* **B371** (1992) 141.

[40] B. Kniehl and A. Sirlin, *On the effect of the $t\bar{t}$ threshold on electroweak parameters*, *Phys. Rev.* **D47** (1993) 883.

[41] A. Stremplat, *Zwei-Schleifen-Beiträge zu leptonischen Präzisionsobservablen*, 1998. Karlsruhe Institute of Technology, Diplomarbeit, see: `http://www.itp.kit.edu/diplomatheses.de.shtml`.

[42] A. Freitas, W. Hollik, W. Walter, and G. Weiglein, *Complete fermionic two loop results for the $M_W - M_Z$ interdependence*, *Phys.Lett.* **B495** (2000) 338–346, [hep-ph/0007091]. [Erratum-ibid. **B570** (2003) 260-264].

[43] A. Freitas, W. Hollik, W. Walter, and G. Weiglein, *Electroweak two loop corrections to the $M_W - M_Z$ mass correlation in the standard model*, *Nucl.Phys.* **B632** (2002) 189–218, [hep-ph/0202131]. [Erratum-ibid. **B666** (2003) 305-307].

[44] M. Awramik and M. Czakon, *Complete two loop electroweak contributions to the muon lifetime in the standard model*, *Phys. Lett.* **B568** (2003) 48, [hep-ph/0305248].

[45] M. Awramik and M. Czakon, *Complete two loop bosonic contributions to the muon lifetime in the standard model*, *Phys. Rev. Lett.* **89** (2002) 241801, [hep-ph/0208113].

[46] A. Onishchenko and O. Veretin, *Two-loop bosonic electroweak corrections to the muon lifetime and $M_W - M_Z$ interdependence*, *Phys. Lett.* **B551** (2003) 111, [hep-ph/0209010].

[47] M. Awramik, M. Czakon, A. Onishchenko, and O. Veretin, *Bosonic corrections to Δr at the two loop level*, *Phys. Rev.* **D68** (2003) 053004, [hep-ph/0209084].

[48] L. Avdeev, J. Fleischer, S. Mikhailov, and O. Tarasov, *$\mathcal{O}(\alpha\alpha_s^2)$ correction to the electroweak ρ parameter*, *Phys.Lett.* **B336** (1994) 560, [hep-ph/9406363].

[49] K. G. Chetyrkin, J. H. Kuhn, and M. Steinhauser, *Corrections of order $\mathcal{O}(G_F M_t^2 \alpha_s^2)$ to the ρ parameter*, *Phys. Lett.* **B351** (1995) 331, [hep-ph/9502291].

[50] K. G. Chetyrkin, J. Kuhn, and M. Steinhauser, *QCD corrections from top quark to relations between electroweak parameters to order α_s^2*, *Phys. Rev. Lett.* **75** (1995) 3394, [hep-ph/9504413].

[51] K. Chetyrkin, J. Kuhn, and M. Steinhauser, *Three loop polarization function and $\mathcal{O}(\alpha_s^2)$ corrections to the production of heavy quarks*, *Nucl.Phys.* **B482** (1996) 213, [hep-ph/9606230].

[52] M. Faisst, J. H. Kuhn, T. Seidensticker, and O. Veretin, *Three loop top quark contributions to the ρ parameter*, *Nucl. Phys.* **B665** (2003) 649, [hep-ph/0302275].

[53] J. van der Bij, K. Chetyrkin, M. Faisst, G. Jikia, and T. Seidensticker, *Three loop leading top mass contributions to the ρ parameter*, *Phys.Lett.* **B498** (2001) 156–162, [hep-ph/0011373].

[54] R. Boughezal, J. Tausk, and J. van der Bij, *Three-loop electroweak correction to the ρ parameter in the large Higgs mass limit*, *Nucl.Phys.* **B713** (2005) 278–290, [hep-ph/0410216].

[55] R. Boughezal and M. Czakon, *Single scale tadpoles and $\mathcal{O}(G_F m_t^2 \alpha_s^3)$ corrections to the ρ parameter*, *Nucl.Phys.* **B755** (2006) 221, [hep-ph/0606232].

[56] K. Chetyrkin, M. Faisst, J. H. Kuhn, P. Maierhofer, and C. Sturm, *Four-Loop QCD Corrections to the ρ Parameter*, *Phys.Rev.Lett.* **97** (2006) 102003, [hep-ph/0605201].

[57] Y. Schroder and M. Steinhauser, *Four-loop singlet contribution to the rho parameter*, *Phys.Lett.* **B622** (2005) 124–130, [hep-ph/0504055].

[58] M. Awramik, M. Czakon, A. Freitas, and G. Weiglein, *Precise prediction for the W boson mass in the standard model*, *Phys.Rev.* **D69** (2004) 053006, [hep-ph/0311148].

[59] M. Awramik, M. Czakon, and A. Freitas, *Electroweak two-loop corrections to the effective weak mixing angle*, *JHEP* **11** (2006) 048, [hep-ph/0608099].

[60] **ATLAS, CMS** Collaborations, *Combined Measurement of the Higgs Boson Mass in pp Collisions at $\sqrt{s} = 7$ and 8 TeV with the ATLAS and CMS Experiments*, *Phys.Rev.Lett.* **114** (2015) 191803, [arXiv:1503.07589].

[61] S. Heinemeyer, W. Hollik, G. Weiglein, and L. Zeune, *Implications of LHC search results on the W boson mass prediction in the MSSM*, *JHEP* **1312** (2013) 084, [arXiv:1311.1663].

[62] R. Barbieri and L. Maiani, *Renormalization of the Electroweak ρ Parameter from Supersymmetric Particles*, *Nucl.Phys.* **B224** (1983) 32.

[63] C. Lim, T. Inami, and N. Sakai, *The ρ Parameter in Supersymmetric Models*, *Phys.Rev.* **D29** (1984) 1488.

[64] E. Eliasson, *Radiative Corrections to Electroweak Interactions in Supergravity GUTs*, *Phys.Lett.* **B147** (1984) 65.

[65] Z. Hioki, *One Loop Effects of Heavy Scalar Quarks in Supersymmetric Electroweak Theory*, *Prog.Theor.Phys.* **73** (1985) 1283.

[66] J. Grifols and J. Sola, *One Loop Renormalization of the Electroweak Parameters in $N = 1$ Supersymmetry*, *Nucl.Phys.* **B253** (1985) 47.

[67] R. Barbieri, M. Frigeni, F. Giuliani, and H. Haber, *Precision Measurements in Electroweak Physics and Supersymmetry*, *Nucl.Phys.* **B341** (1990) 309–321.

[68] M. Drees and K. Hagiwara, *Supersymmetric Contribution to the Electroweak ρ Parameter*, *Phys.Rev.* **D42** (1990) 1709–1725.

[69] M. Drees, K. Hagiwara, and A. Yamada, *Process independent radiative corrections in the minimal supersymmetric standard model*, *Phys.Rev.* **D45** (1992) 1725–1743.

[70] P. H. Chankowski, A. Dabelstein, W. Hollik, W. Mosle, S. Pokorski, and J. Rosiek, *Δr in the MSSM*, *Nucl.Phys.* **B417** (1994) 101.

[71] D. Garcia and J. Sola, *Full one loop supersymmetric quantum effects on M_W*, *Mod.Phys.Lett.* **A9** (1994) 211–224.

[72] D. M. Pierce, J. A. Bagger, K. T. Matchev, and R.-j. Zhang, *Precision corrections in the minimal supersymmetric standard model*, *Nucl.Phys.* **B491** (1997) 3–67, [hep-ph/9606211].

[73] S. Heinemeyer, W. Hollik, D. Stöckinger, A. M. Weber, and G. Weiglein, *Precise prediction for M_W in the MSSM*, *JHEP* **08** (2006) 052, [hep-ph/0604147].

[74] A. Djouadi, P. Gambino, S. Heinemeyer, W. Hollik, C. Junger, and G. Weiglein, *Supersymmetric contributions to electroweak precision observables: QCD corrections*, *Phys.Rev.Lett.* **78** (1997) 3626, [hep-ph/9612363].

[75] A. Djouadi, P. Gambino, S. Heinemeyer, W. Hollik, C. Junger, and G. Weiglein, *Leading QCD corrections to scalar quark contributions to electroweak precision observables*, *Phys.Rev.* **D57** (1998) 4179, [hep-ph/9710438].

[76] S. Heinemeyer and G. Weiglein, *Leading electroweak two loop corrections to precision observables in the MSSM*, *JHEP* **0210** (2002) 072, [hep-ph/0209305].

[77] J. Haestier, S. Heinemeyer, D. Stöckinger, and G. Weiglein, *Electroweak precision observables: Two-loop Yukawa corrections of supersymmetric particles*, *JHEP* **0512** (2005) 027, [hep-ph/0508139].

[78] F. Domingo and T. Lenz, *W mass and Leptonic Z-decays in the NMSSM*, *JHEP* **1107** (2011) 101, [arXiv:1101.4758].

[79] J. Cao and J. M. Yang, *Anomaly of $Zb\bar{b}$ coupling revisited in MSSM and NMSSM*, *JHEP* **0812** (2008) 006, [arXiv:0810.0751].

[80] J. Cao, Z. Heng, and J. M. Yang, *Rare Z-decay into light CP-odd Higgs bosons: a comparative study in different new physics models*, *JHEP* **1011** (2010) 110, [arXiv:1007.1918].

[81] S. P. Martin, *A Supersymmetry primer*, hep-ph/9709356.

[82] **Particle Data Group**, K. Olive, et al., *Review of Particle Physics*, *Chin.Phys.* **C38** (2014) 090001.

[83] R. Behrends, R. Finkelstein, and A. Sirlin, *Radiative corrections to decay processes*, *Phys.Rev.* **101** (1956) 866–873.

[84] T. Kinoshita and A. Sirlin, *Radiative corrections to Fermi interactions*, *Phys.Rev.* **113** (1959) 1652–1660.

[85] T. van Ritbergen and R. G. Stuart, *On the precise determination of the Fermi coupling constant from the muon lifetime*, *Nucl.Phys.* **B564** (2000) 343–390, [hep-ph/9904240].

[86] M. Steinhauser and T. Seidensticker, *Second order corrections to the muon lifetime and the semileptonic B decay*, *Phys.Lett.* **B467** (1999) 271–278, [hep-ph/9909436].

[87] A. Pak and A. Czarnecki, *Mass effects in muon and semileptonic $b \to c$ decays*, *Phys.Rev.Lett.* **100** (2008) 241807, [arXiv:0803.0960].

[88] **MuLan** Collaboration, D. Webber et al., *Measurement of the Positive Muon Lifetime and Determination of the Fermi Constant to Part-per-Million Precision*, *Phys.Rev.Lett.* **106** (2011) 041803, [arXiv:1010.0991].

[89] J. Küblbeck, M. Böhm, and A. Denner, *Feyn Arts: Computer Algebraic Generation of Feynman Graphs and Amplitudes*, *Comput.Phys.Commun.* **60** (1990) 165–180.

[90] A. Denner, H. Eck, O. Hahn, and J. Küblbeck, *Compact Feynman rules for Majorana fermions*, *Phys.Lett.* **B291** (1992) 278–280.

[91] A. Denner, H. Eck, O. Hahn, and J. Küblbeck, *Feynman rules for fermion number violating interactions*, *Nucl.Phys.* **B387** (1992) 467–484.

[92] J. Küblbeck, H. Eck, and R. Mertig, *Computeralgebraic generation and calculation of Feynman graphs using FeynArts and FeynCalc*, *Nucl.Phys.Proc.Suppl.* **29A** (1992) 204–208.

[93] T. Hahn, *Generating Feynman diagrams and amplitudes with FeynArts 3*, *Comput.Phys.Commun.* **140** (2001) 418, [hep-ph/0012260].

[94] T. Hahn and C. Schappacher, *The Implementation of the Minimal Supersymmetric Standard model in FeynArts and FormCalc*, *Comput.Phys.Commun.* **143** (2002) 54–68, [hep-ph/0105349].

[95] M. Veltman, *Limit on Mass Differences in the Weinberg Model*, *Nucl.Phys.* **B123** (1977) 89.

[96] T. Hahn and M. Perez-Victoria, *Automatized one loop calculations in four-dimensions and D-dimensions*, *Comput.Phys.Commun.* **118** (1999) 153–165, [hep-ph/9807565].

[97] F. Staub, T. Ohl, W. Porod, and C. Speckner, *A Tool Box for Implementing Supersymmetric Models*, *Comput.Phys.Commun.* **183** (2012) 2165–2206, [arXiv:1109.5147].

[98] F. Staub, *SARAH*, arXiv:0806.0538.

[99] L. Zeune, *Precise predictions for the W boson mass in models beyond the Standard Model*, 2011. University of Göttingen, Diplomarbeit, see: http://physik2.uni-goettingen.de/research/high-energy/publications/.

[100] D. Y. Bardin, A. Leike, T. Riemann, and M. Sachwitz, *Energy dependent width effects in e^+e^- annihilation near the Z pole*, *Phys. Lett.* **B206** (1988) 539.

[101] S. P. Martin, *Pole mass of the W boson at two-loop order in the pure $\overline{MS}$ scheme*, *Phys.Rev.* **D91** (2015), no. 11 114003, [arXiv:1503.03782].

[102] S. P. Martin, *Z boson pole mass at two-loop order in the pure MS-bar scheme*, arXiv:1505.04833.

[103] M. Consoli, W. Hollik, and F. Jegerlehner, *The Effect of the Top Quark on the $M_W - M_Z$ Interdependence and Possible Decoupling of Heavy Fermions from Low-Energy Physics*, *Phys.Lett.* **B227** (1989) 167.

[104] T. Hahn, S. Heinemeyer, W. Hollik, H. Rzehak, and G. Weiglein, *FeynHiggs: A program for the calculation of MSSM Higgs-boson observables - Version 2.6.5*, *Comput.Phys.Commun.* **180** (2009) 1426–1427.

[105] M. Frank, T. Hahn, S. Heinemeyer, W. Hollik, H. Rzehak, et al., *The Higgs Boson Masses and Mixings of the Complex MSSM in the Feynman-Diagrammatic Approach*, *JHEP* **0702** (2007) 047, [hep-ph/0611326].

[106] G. Degrassi, S. Heinemeyer, W. Hollik, P. Slavich, and G. Weiglein, *Towards high precision predictions for the MSSM Higgs sector*, *Eur.Phys.J.* **C28** (2003) 133–143, [hep-ph/0212020].

[107] S. Heinemeyer, W. Hollik, and G. Weiglein, *The Masses of the neutral CP even Higgs bosons in the MSSM: Accurate analysis at the two loop level*, *Eur.Phys.J.* **C9** (1999) 343–366, [hep-ph/9812472].

[108] S. Heinemeyer, W. Hollik, and G. Weiglein, *FeynHiggs: A Program for the calculation of the masses of the neutral CP even Higgs bosons in the MSSM*, *Comput.Phys.Commun.* **124** (2000) 76–89, [hep-ph/9812320].

[109] R. Barbieri, M. Beccaria, P. Ciafaloni, G. Curci, and A. Vicere, *Two loop heavy top effects in the Standard Model*, *Nucl.Phys.* **B409** (1993) 105–127.

[110] J. Fleischer, O. Tarasov, and F. Jegerlehner, *Two loop heavy top corrections to the ρ parameter: A Simple formula valid for arbitrary Higgs mass*, *Phys.Lett.* **B319** (1993) 249–256.

[111] U. Ellwanger, J. F. Gunion, and C. Hugonie, *NMHDECAY: A Fortran code for the Higgs masses, couplings and decay widths in the NMSSM*, *JHEP* **0502** (2005) 066, [hep-ph/0406215].

[112] U. Ellwanger and C. Hugonie, *NMHDECAY 2.0: An Updated program for sparticle masses, Higgs masses, couplings and decay widths in the NMSSM*, *Comput.Phys.Commun.* **175** (2006) 290–303, [hep-ph/0508022].

[113] G. Belanger, F. Boudjema, C. Hugonie, A. Pukhov, and A. Semenov, *Relic density of dark matter in the NMSSM*, *JCAP* **0509** (2005) 001, [hep-ph/0505142].

[114] U. Ellwanger and C. Hugonie, *NMSPEC: A Fortran code for the sparticle and Higgs masses in the NMSSM with GUT scale boundary conditions*, *Comput.Phys.Commun.* **177** (2007) 399–407, [hep-ph/0612134].

[115] J. Baglio, R. Gröber, M. Mühlleitner, D. Nhung, H. Rzehak, et al., *NMSSMCALC: A Program Package for the Calculation of Loop-Corrected Higgs Boson Masses and Decay Widths in the (Complex) NMSSM*, *Comput.Phys.Commun.* **185** (2014), no. 12 3372–3391, [arXiv:1312.4788].

[116] M. Goodsell, K. Nickel, and F. Staub, *Two-loop Higgs mass calculation from a diagrammatic approach*, arXiv:1503.03098.

[117] P. Drechsel, L. Galeta, S. Heinemeyer, and G. Weiglein, *In preparation*, DESY 15-069.

[118] K. E. Williams, H. Rzehak, and G. Weiglein, *Higher order corrections to Higgs boson decays in the MSSM with complex parameters*, *Eur.Phys.J.* **C71** (2011) 1669, [arXiv:1103.1335].

[119] See: http://www.th.u-psud.fr/NMHDECAY/README.

[120] P. Bechtle, O. Brein, S. Heinemeyer, O. Stål, T. Stefaniak, et al., HiggsBounds – 4*: Improved Tests of Extended Higgs Sectors against Exclusion Bounds from LEP, the Tevatron and the LHC*, *Eur.Phys.J.* **C74** (2014), no. 3 2693, [arXiv:1311.0055].

[121] P. Bechtle, O. Brein, S. Heinemeyer, O. Stal, T. Stefaniak, et al., *Recent Developments in HiggsBounds and a Preview of HiggsSignals*, *PoS* **CHARGED2012** (2012) 024, [arXiv:1301.2345].

[122] P. Bechtle, O. Brein, S. Heinemeyer, G. Weiglein, and K. E. Williams, *HiggsBounds 2.0.0: Confronting Neutral and Charged Higgs Sector Predictions with Exclusion Bounds from LEP and the Tevatron*, *Comput.Phys.Commun.* **182** (2011) 2605–2631, [arXiv:1102.1898].

[123] P. Bechtle, O. Brein, S. Heinemeyer, G. Weiglein, and K. E. Williams, *HiggsBounds: Confronting Arbitrary Higgs Sectors with Exclusion Bounds from LEP and the Tevatron*, *Comput.Phys.Commun.* **181** (2010) 138–167, [arXiv:0811.4169].

[124] **Particle Data Group**, J. Beringer, et al., *Review of Particle Physics (RPP)*, *Phys.Rev.* **D86** (2012) 010001. And 2013 partial update for the 2014 edition.

[125] R. Mahbubani, M. Papucci, G. Perez, J. T. Ruderman, and A. Weiler, *Light Nondegenerate Squarks at the LHC*, *Phys.Rev.Lett.* **110** (2013), no. 15 151804, [arXiv:1212.3328].

[126] G. Degrassi and P. Slavich, *On the radiative corrections to the neutral Higgs boson masses in the NMSSM*, *Nucl.Phys.* **B825** (2010) 119–150, [arXiv:0907.4682].

[127] S. King, M. Mühlleitner, and R. Nevzorov, *NMSSM Higgs Benchmarks Near 125 GeV*, *Nucl.Phys.* **B860** (2012) 207–244, [arXiv:1201.2671].

[128] M. Carena, S. Heinemeyer, O. Stål, C. Wagner, and G. Weiglein, *MSSM Higgs Boson Searches at the LHC: Benchmark Scenarios after the Discovery of a Higgs-like Particle*, *Eur. Phys. J.* **C73** (2013) 2552, [arXiv:1302.7033].

[129] **ATLAS** Collaboration, G. Aad et al., *Search for charged Higgs bosons decaying via $H^{\pm} \to \tau^{\pm}\nu$ in fully hadronic final states using pp collision data at $\sqrt{s} = 8$ TeV with the ATLAS detector*, *JHEP* **1503** (2015) 088, [arXiv:1412.6663].

[130] **CMS** Collaboration. CMS-PAS-HIG-14-020.

[131] M. E. Peskin and T. Takeuchi, *A New constraint on a strongly interacting Higgs sector*, *Phys.Rev.Lett.* **65** (1990) 964–967.

[132] W. J. Marciano and J. L. Rosner, *Atomic parity violation as a probe of new physics*, *Phys.Rev.Lett.* **65** (1990) 2963–2966. [Erratum-ibid. **68** (1992) 898].